

# Comparative study of Higgs transition in one-component and two-component lattice superconductor models

Olexei I. Motrunich

*Department of Physics, California Institute of Technology, Pasadena, CA 91125*

Ashvin Vishwanath

*Department of Physics, University of California, Berkeley, CA 94720*

*Materials Sciences Division, Lawrence Berkeley National Laboratory, Berkeley, CA 94720*

(Dated: November 12, 2018)

Using Monte Carlo simulations, we study a Higgs transition in several three-dimensional lattice realizations of the noncompact  $CP^1$  model (NCCP<sup>1</sup>), a gauge theory with two complex matter fields with  $SU(2)$  invariance. By comparing with a one-component theory, which is well understood and has continuous transition in the inverted XY universality class, we argue that the two-component case also has continuous Higgs transition with a larger correlation length exponent (i.e., it is “more continuous”). The transition can become first order in the vicinity of a new “Molecular” phase, which occurs in one of our models, but is continuous in a wide range of parameters away from this phase. The situation is significantly clarified by studying a model where the Molecular phase is entirely absent, and a wide regime with a continuous transition can be readily established. The two-component theory is also an effective description of the hedgehog-suppressed  $O(3)$  universality, and results are relevant for the recently discussed “deconfined quantum criticality” scenario for the continuous Valence Bond Solid to Neel quantum phase transition.

## I. INTRODUCTION

In this paper, we examine the nature of the Higgs transition in a two-component theory with a dynamical gauge field in three (classical) dimensions (3D).<sup>1</sup> A schematic continuum action is

$$S = \int_{R^3} |(\nabla - i\mathbf{a})\Psi|^2 + m|\Psi|^2 + u|\Psi|^4 + \kappa(\nabla \times \mathbf{a})^2. \quad (1)$$

$\Psi$  has two complex components and  $\mathbf{a}$  is the gauge field that can take any real values (i.e., it is non-compact). This theory is also called the noncompact  $CP^1$  model (NCCP<sup>1</sup>).<sup>2</sup> When the charged field  $\Psi$  is gapped, the gauge field is massless and there is a free photon, but when  $\Psi$  condenses,  $\mathbf{a}$  becomes massive – this is the Higgs transition. In Ref. 2, we argued that this action also describes an  $O(3)$  classical spin system with prohibited hedgehog topological defects on long scales. In particular, the ordering transition in the hedgehog-suppressed model and the above Higgs transition are in the same universality. The nature of the transition is of interest in the context of the recently discussed quantum phase transitions that lie outside the Landau-Ginzburg-Wilson framework.<sup>3,4,5,6,7</sup> Thus, it has been proposed<sup>3,4,5,6</sup> that the Neel to Valence Bond Solid transition in a spin-1/2 system with  $SU(2)$  symmetry can undergo a continuous quantum phase transition described by the same universality Eq. (1).

Here we present a detailed numerical analysis of several lattice realizations of the theory (1) (we will refer to these as lattice superconductor models<sup>8</sup>). We extend the study of Ref. 2 of the  $SU(2)$ -symmetric two-component model, with the goal to check more thoroughly the proposed second-order nature of the transition. Here, we argue that our models have continuous Higgs transition

over wide parameter ranges, see Figs. 1b,c. Note that in one of our models, Fig. 1b, we also find a parameter range, in the vicinity of a third “Molecular” phase [produced when gauge neutral pairs of the  $\Psi_i$  particles of Eq. (1) condense], where the transition becomes first order. This is always a possibility, and in the specific model happens generically near this new phase. We adopt two fresh strategies to establish the nature of the transition in these systems. First, in the regime where we believe the transition is second-order, we compare with a one-component model for which it is well established that the transition is continuous,<sup>8</sup> and show that the transition in our two-component models is “more continuous”, in the sense that the thermodynamic singularities are more weak. Second, we introduce a lattice realization of the model in Eq. (1), where the Molecular phase is entirely absent. The Higgs transition is then shown to be continuous over the entire phase boundary, which greatly simplifies the interpretation. Our best estimates for the exponents at this transition are  $\nu = 0.7 - 0.75$  and  $\eta = 0.2 - 0.4$ . Recent Quantum Monte Carlo simulations of square lattice  $S = 1/2$  Heisenberg antiferromagnets with four spin exchange terms and  $SU(2)$  symmetry have also found a continuous relativistic transition between a Neel and Valence Bond Solid phase,<sup>5,6</sup> which is believed to be in the same universality class as the transition studied here. The exponents obtained in those studies are  $\eta = 0.26(3)$  and  $\nu = 0.78(3)$  in Ref. 5 and  $\eta = 0.35(3)$ ,  $\nu = 0.68(4)$  in Ref. 6, consistent with the ones reported here.

Other studies,<sup>9,10,11</sup> particularly in two-component superconductor models where the  $SU(2)$  symmetry is broken down to  $U(1)$  (easy plane NCCP<sup>1</sup>), have suggested that such Higgs transitions may always be first order. While those authors so far have found first order tran-

sitions in these  $U(1)\times U(1)$  models, we do not know any fundamental reasons why this needs to hold generally. This is particularly true in light of the evidence presented here for a continuous transition in the  $SU(2)$  symmetric model. Moreover, the studies in Refs. 9,10 were performed on models where the Molecular phase is present, which we suspect may be driving the first order nature of the transition. In future work we will apply the ideas described here to obtain and study models without a Molecular phase in this symmetry class as well, which should help clarify the issue.

The study of the criticality in the theory (1) dates back to Halperin, Lubensky, and Ma.<sup>1</sup> At the fixed point where the matter and gauge fields are decoupled ( $e^2 \sim 1/\kappa \rightarrow 0$ ), the gauge interaction is a relevant perturbation, and no new stable fixed points were found in  $d = 4 - \epsilon$  treatment when the number of components  $N$  is less than 365. This was interpreted as an evidence for a fluctuation-induced first-order transition. For larger  $N$ , and also in a  $1/N$  treatment directly in  $d = 3$ , the transition was found to be continuous. Later work by Dasgupta and Halperin<sup>8</sup> showed that the transition in the  $N = 1$  case can also be continuous. The one-component superconductor model is dual to the usual 3D XY model that has only short-range interactions. Concisely stated, one can fruitfully think about the one-component system in terms of the Abrikosov-Nielsen-Olesen (ANO) vortices which carry quantized gauge flux and have only short-range interactions. The duality claim then follows if we recall that the 3D XY model can be also viewed as a system of short-range interacting current loops. The Higgs phase where the ANO vortices are gapped corresponds to the disordered phase of the XY model with small loops, while the disordered phase of the charged superconductor where the ANO vortices condense corresponds to the ordered phase of the XY model with proliferated loops. Thus, the ANO vortices play a crucial role, which is difficult to capture in the  $4 - \epsilon$  treatment. We expect that the same physics happens in the two-component case, but with the ANO vortices that now have non-trivial internal structure. While our analytical picture is not as complete as in the one-component case, since we are unable to perform a duality transformation in the present case, one of our models has a limit that strongly suggests such an interpretation, and we confirm that the transition is continuous by direct Monte Carlo studies on the lattice.

One of our main strategy exploring such new two-component matter - gauge systems in Monte Carlo is to compare closely with the well-understood one-component case. We simulate both systems under similar conditions and compare directly observables in the gauge sector that detect the Meissner-Anderson-Higgs physics of charged condensates. We also study separately new features in the two-component system, such as the presence and possible condensation of composite gauge-neutral fields.

The paper is organized as follows. In Sec. II, we define the models and describe their overall phase diagrams. In

Sec. III, we focus on the Higgs transitions and present several two-component cases where we argue the transition is continuous. We also discuss the observed systematics along the full Photon to Higgs phase boundary and show that we can improve it by suppressing possible other phases. In Sec. IV, we summarize the results and conclude with an outlook.

## II. MODELS AND THEIR PHASE DIAGRAMS

We study the following three models. The first model realizes a one-component lattice superconductor:

$$S_{\text{NCCP}^0} = -\mathcal{J} \sum_{i,\mu} \cos(\theta_i - \theta_{i+\hat{\mu}} + a_{i\mu}) + S_a, \quad (2)$$

$$S_a = \frac{\mathcal{K}}{2} \sum_{\square} (\Delta \times a)^2. \quad (3)$$

A  $U(1)$  matter field  $e^{i\theta}$  resides on the sites of a 3D cubic lattice, while a non-compact gauge field  $a_\mu$  resides on the links;  $S_a$  is the usual lattice Maxwell action for the gauge field. We will use ‘NCCP<sup>0</sup>’ as a short-hand reference to this model, where ‘CP<sup>0</sup>’ refers to one matter field component while ‘NC’ emphasizes that the gauge field is non-compact.<sup>2,3</sup> This model and the ones below have two parameters  $\mathcal{J}$  and  $\mathcal{K}$ . The NCCP<sup>0</sup> model is our reference system for matter-gauge simulations.

The second model realizes a two-component lattice superconductor:

$$S_{\text{NCCP}^1, \text{model I}} = -\frac{\mathcal{J}}{2} \sum_{i,\mu} \left( \mathbf{z}_i^\dagger \mathbf{z}_{i+\hat{\mu}} e^{ia_{i\mu}} + c.c. \right) + S_a. \quad (4)$$

Here the matter field is a  $CP^1$  field  $\mathbf{z} = (z_\uparrow, z_\downarrow)$ ,  $|\mathbf{z}| = 1$ . This model was introduced in Ref. 2 and studied at  $\mathcal{K} = 0.6$  using small system sizes; the present work is an extension of that study.

The third model is a different realization of the two-component case:

$$S_{\text{NCCP}^1, \text{model II}} = S_{\text{NCCP}^1, \text{model I}} + \sum_{i,\mu} \ln I_0(\mathcal{J} |\mathbf{z}_i^\dagger \mathbf{z}_{i+\hat{\mu}}|). \quad (5)$$

Here  $I_0(x)$  is the modified Bessel function. Compared to the model I, there is an additional antiferromagnetic interaction between nearest-neighbor spins. This interaction eliminates the unwanted ‘Molecular’ phase from our phase diagram. Our motivation for this model will become clear soon, while here we only note that the specific form allows some analytical understanding of the phase diagram and that any such short-range interaction that respects the symmetries of the problem does not change the universality of the transition.

Figure 1 shows the phase diagrams of the three models in the  $\mathcal{K} - \mathcal{J}$  parameter space. In each case, for small  $\mathcal{J}$ , the matter fields are gapped and the gauge field is massless described by the Maxwell term – we mark this

as the Photon phase. On the other hand, when  $\mathcal{J}$  and  $\mathcal{K}$  are sufficiently large, the matter fields condense and gap out the photon – this is the Higgs phase. In the one-component case, there remain no gapless excitations. In the two-component system, we can construct a gauge-invariant O(3) vector field

$$\vec{n} = \mathbf{z}^\dagger \vec{\sigma} \mathbf{z} . \quad (6)$$

This obtains an expectation value in the Higgs phase, and there appear Goldstone modes associated with the global symmetry breaking. The focus in this paper is on the Photon to Higgs transition driven by the condensation of the charged matter fields. We will also see how to view this transition coming from the Higgs side as driven by proliferation of the ANO vortices with internal structure.

Proceeding with more details on the phase diagrams, consider first the NCCP<sup>0</sup> model. At  $\mathcal{K} = \infty$ , there is no gauge field left and the transition along this axis is 3D XY ordering of the  $e^{i\theta}$  field (in Fig. 1a, this transition point is indicated with a star symbol). When  $\mathcal{K}$  becomes finite and the matter-gauge coupling is switched on, the universality of the transition changes. Dasgupta and Halperin<sup>8</sup> argued that sufficiently far from the  $\mathcal{K} = \infty$  limit, the transition becomes inverted XY as summarized in Sec. I in terms of the ANO vortices. We are also mostly interested in moderate  $\mathcal{K}$ . Using classical Monte Carlo, we studied several points along the phase boundary and found continuous transitions in our model; these points are indicated with open symbols. (The limit of large but finite  $\mathcal{K}$  was not answered in Ref. 8, but several scenarios were discussed. One possibility is that the whole line is described by the inverted XY universality.)

The picture of the transition becomes particularly simple in the limit  $\mathcal{J} = \infty$ . Here, the gauge field takes on  $2\pi$ -integer values and the model reduces to that of conserved discrete-valued fluxes  $B_\mu = (\nabla \times a)_\mu$  with steric interactions,

$$Z_{\text{NCCP}^0}^{\mathcal{J}=\infty} = \sum_{\mathbf{B}=2\pi \times \text{int}, \nabla \cdot \mathbf{B}=0, \mathbf{B}_{\text{tot}}=0} \exp \left[ -\frac{\mathcal{K}}{2} \sum_{\square} B^2 \right] . \quad (7)$$

This is the familiar loop representation of the 3D XY model and has been studied in great detail in the literature. Note that in our ensemble derived from the gauge model the total flux is constrained to be zero, but this is not important in the thermodynamic limit. There are only small loops for  $\mathcal{K} > \mathcal{K}_c = 0.07606$ , but they proliferate for  $\mathcal{K} < \mathcal{K}_c$ . The transition is 3D XY in terms of these short-range interacting loops, which are precisely the ANO vortices carrying quantized flux. These loops are gapped on the Higgs side and condense upon reducing  $\mathcal{K}$  and  $\mathcal{J}$ , which is why the transition is referred to as ‘inverted XY’ (as opposed to ‘direct XY’ transition at  $\mathcal{K} = \infty$  where currents conjugate to  $e^{i\theta}$  proliferate upon increasing  $\mathcal{J}$ ). The universality of the transition remains unchanged also away from the  $\mathcal{J} = \infty$  limit. Indeed, one can see that finite  $\mathcal{J}$  only leads to short-range modifications of the ANO vortex interactions and therefore does

not change the nature of the transition. To conclude the description of the NCCP<sup>0</sup> phase diagram, we readily see that there are no transitions along the  $\mathcal{K} = 0$  or  $\mathcal{J} = 0$  axes in Fig. 1a.

Consider now the NCCP<sup>1</sup> model I, whose phase diagram is shown in Fig. 1b. Similarly to the NCCP<sup>0</sup> case, there is no transition along the  $\mathcal{J} = 0$  axis. Along the  $\mathcal{K} = \infty$  line, the gauge field is again absent and the transition is in the O(4) universality class, but the universality changes once  $\mathcal{K}$  becomes finite. The region where we find the transition is continuous in a new universality class is marked with open symbols in the figure (details of the numerical study of the transitions are given in Sec. III).

Unlike the one-component case, this two-component model has an additional phase at small  $\mathcal{K}$  and large  $\mathcal{J}$ , which, while interesting on its own, does not bear on the universality class of the Higgs transition that we are interested in. For completeness and in order to better understand the numerics in this model, let us describe the new phase, which we mark as Molecular. Here, the charged field  $\mathbf{z}$  is gapped but the charge-neutral field  $\vec{n}$  obtains an expectation value, and the O(3) order and the photon coexist. This molecular condensate appears because of the attraction between oppositely charged  $\mathbf{z}^\dagger$  and  $\mathbf{z}$  fields. Explicitly, consider the  $\mathcal{K} = 0$  axis. The gauge field can be integrated out completely, with the resulting action for the  $\mathbf{z}$ ’s

$$S_{\text{NCCP}^1, \text{model I}}^{\mathcal{K}=0}[\mathbf{z}] = - \sum_{i,\mu} \ln I_0(\mathcal{J} |\mathbf{z}_i^\dagger \mathbf{z}_{i+\mu}|) . \quad (8)$$

Since

$$|\mathbf{z}_i^\dagger \mathbf{z}_j| = \sqrt{\frac{1 + \vec{n}_i \cdot \vec{n}_j}{2}} , \quad (9)$$

there is thus a ferromagnetic interaction between neighboring spins that drives an O(3) ordering transition upon increasing  $\mathcal{J}$  along the  $\mathcal{K} = 0$  axis. The transition remains in the same universality also for small  $\mathcal{K}$ . Since the condensate is neutral, the photon remains free and is a harmless spectator across this Photon - Molecular phase transition.

Consider now the transition from the Molecular to the Higgs phase at large  $\mathcal{J}$ . This is similar to the one-component transition described earlier. Indeed, if we take an ordered state of the  $\vec{n}$ ’s, the remaining U(1) phase degrees of freedom of  $\mathbf{z}$ ’s are coupled to the gauge field in the same manner as the  $e^{i\theta}$ ’s in Eq. (3), and the Molecular to Higgs phase transition is the condensation of this charged field. In particular, the transition at  $\mathcal{J} = \infty$  occurs at the same  $\mathcal{K}_c$  and is in the inverted 3D XY class; the transition is expected to remain in this universality also away from the  $\mathcal{J} = \infty$  limit. The Goldstone modes of the broken global O(3) are present both in the Molecular and Higgs phases and are harmless spectators across this transition.

Having discussed the three phases, consider now the region where they meet – the ‘fork’ in the phase diagram. A

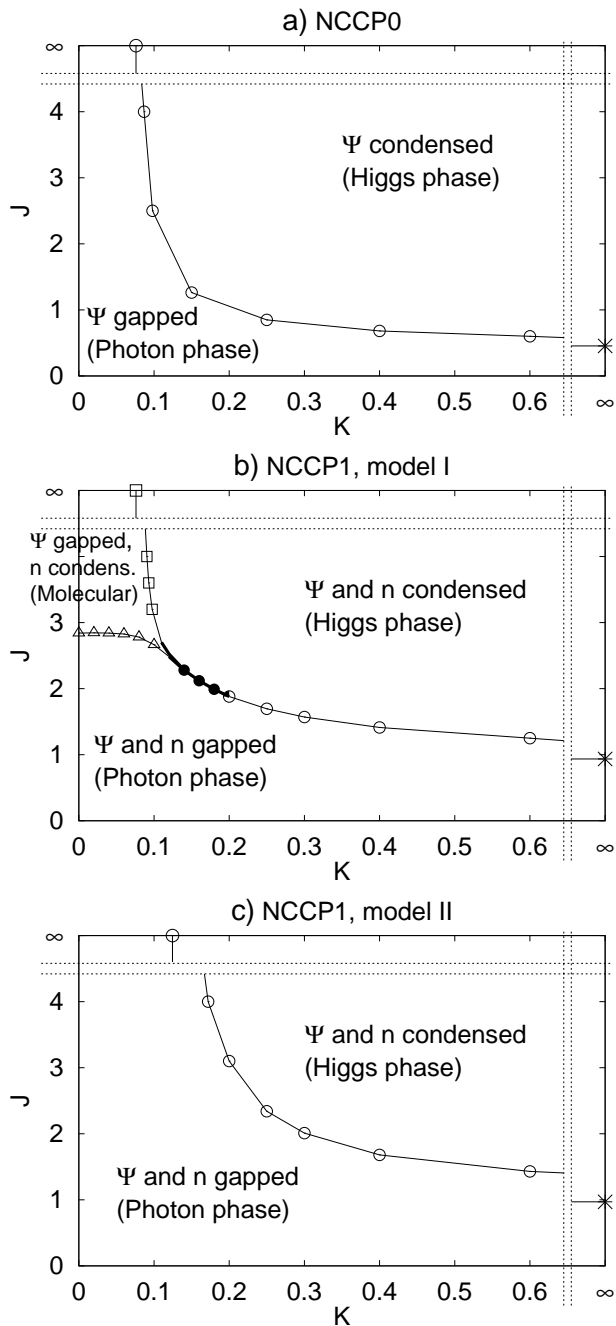


FIG. 1: Phase diagrams of the three models. In the NCCP<sup>0</sup> model,  $\Psi = e^{i\theta}$ , while in the NCCP<sup>1</sup> case,  $\Psi = \mathbf{z} = (z_{\uparrow}, z_{\downarrow})$  is a two-component field. a) The transition between the Photon and Higgs phases is inverted XY and is denoted with open symbols, except at  $\mathcal{K} = \infty$  where it is direct XY (denoted with star). b) NCCP<sup>1</sup> model I has a rich phase diagram which contains also the Molecular phase where  $\Psi$  is gapped but  $\vec{n}$  orders. Our main interest is on the Photon to Higgs phase transition; the points where it is continuous are denoted with open circles, while in the vicinity where the three phases meet the transition becomes first order and is denoted with filled circles. c) The Molecular phase is eliminated in the NCCP<sup>1</sup> model II, allowing to focus solely on the Photon - Higgs transition. We find that everywhere along the phase boundary the transition is continuous (indicated with open symbols).

mean field argument<sup>9</sup> summarized in Appendix A shows that in the immediate vicinity of the fork the Photon to Higgs and Molecular to Higgs transitions become first order, see Fig. 14. The Photon to Molecular transition, on the other hand, remains continuous. Focusing on the Photon to Higgs transition, the first order line terminates at a so-called tricritical point, beyond which the transition is continuous. We indeed find similar picture in the Monte Carlo simulations of the model, where the transition is second-order for the  $\mathcal{K} > 0.2$  points in Fig. 1, and this is the region that we are most interested in. However, as we will describe in Sec. III E, a detailed study of the universality is hampered by the fact that this region is bordered by two different critical points that are not related to the fixed point of our transition: On one hand, the system needs to be sufficiently away from the  $\mathcal{K} = \infty$  limit to depart from the O(4) universality class. On the other hand, it also needs to be far from the first-order end-point that imposes its own crossovers before the system flows to the fixed point that controls the transition we are interested in. Note that the renormalization group flows that we have in mind are in a more general space than the  $\mathcal{K} - \mathcal{J}$  parameter space of the model, so the above scenario is consistent.

Because of these complications, the NCCP<sup>1</sup> model I, while simple to formulate, requires good understanding of all crossovers before interpreting the results. We do not have such a complete control to be able to reliably extract the critical indices, but we will show representative points on the phase boundary where numerics is strongly in favor of the second-order character which is “more continuous” than in the NCCP<sup>0</sup> case. We will further argue for the hypothesis of the tricritical point in this model in Sec. III E.

The universality of the Higgs transition that we want to study is independent of additional short-range interactions as long as the transition remains continuous. In this respect, to better focus on the scaling properties, we also consider the NCCP<sup>1</sup> model II, Eq. (5), where we have added some antiferromagnetic interaction between neighboring spins that hinders the ordering of the  $\vec{n}$ 's. In fact, with the hindsight of Eq. (8), the chosen interaction precisely compensates the ferromagnetic interaction in the original model I along the  $\mathcal{K} = 0$  axis. In particular, the model II has no phase transition along this axis. We actually find that the Molecular phase is eliminated in this model, and the resulting phase diagram is displayed in Fig. 1c. The transition remains continuous all the way to the  $\mathcal{J} = \infty$  limit, and the phase diagram in the  $\mathcal{K} - \mathcal{J}$  plane looks similar to the NCCP<sup>0</sup> case.

Thus, in the NCCP<sup>1</sup> model II, we avoid the complicating crossovers caused by the possible tricritical point in the vicinity of the Molecular phase. We only need to worry about being sufficiently away from the  $\mathcal{K} = \infty$  limit, and this is similar to the NCCP<sup>0</sup> case that we understand analytically and can compare numerically. We expect that adding generic antiferromagnetic interactions between the  $\vec{n}$ 's would give a similar improvement in the

NCCP<sup>1</sup> model, suppressing the Molecular phase, but we have chosen the specific form to avoid possibly introducing new phases in the phase diagram. From a Monte Carlo study of the model II combined with a separate study of the  $\mathcal{J} = \infty$  limit and an analysis of the stability away from this limit, we conclude that no other phase appears in this model.

Let us describe in more detail the  $\mathcal{J} = \infty$  limit, which we formulate as

$$Z_{\text{NCCP}^1, \text{model II}}^{\mathcal{J}=\infty} = \sum_B \int D\mathbf{z} \delta(|\mathbf{z}|^2 = 1) \exp \left[ -\frac{\mathcal{K}}{2} \sum_{\square} (B + \nabla \times \mathcal{A}[\mathbf{z}])^2 \right] \quad (10)$$

Here the primed sum is over  $2\pi$ -integer-valued conserved  $B$ -fluxes as in Eq. (7). The ensemble also contains CP<sup>1</sup> fields  $\mathbf{z}$  residing on the sites and specifying uniquely link variables  $\mathcal{A}$  as follows:

$$e^{i\mathcal{A}_{ij}} = \frac{\mathbf{z}_i^\dagger \mathbf{z}_j}{|\mathbf{z}_i^\dagger \mathbf{z}_j|}. \quad (11)$$

Note that any  $2\pi$  ambiguity in the  $\mathcal{A}$ 's can be absorbed by the  $B$ 's. Crudely, we obtain Eq. (10) by focusing on the phases of the link variables  $\mathbf{z}_i^\dagger \mathbf{z}_j$  while completely suppressing the role of their amplitudes, and this is precisely achieved when we take the  $\mathcal{J} \rightarrow \infty$  limit in the model II.

Comparing with the  $\mathcal{J} = \infty$  limit in the NCCP<sup>0</sup> case, the NCCP<sup>1</sup> variant can be also viewed as a loop model, but the loops have non-trivial internal structure derived from the coupled degrees of freedom  $\mathbf{z}_i$ . Numerically we find that this system has a continuous transition at  $\mathcal{K}_c \approx 0.1245$ , see Sec. III C, and the universality of the transition is different from the loops with no internal structure. We can also carry through an analysis in the model II when  $\mathcal{J}$  is large but finite and find that this leads only to short-range modifications that vanish in the  $\mathcal{J} \rightarrow \infty$  limit (this is similar to how one analyzes the NCCP<sup>0</sup> case at large  $\mathcal{J}$ ). We then propose that the whole phase boundary in Fig. 1c is in the same universality as the transition found in Monte Carlo at  $\mathcal{J} = \infty$ .

### III. COMPARATIVE STUDY OF THE TRANSITIONS

#### A. Monte Carlo measurements. Scaling analysis

We first summarize our numerical measurements. We perform classical Monte Carlo simulations using local updates of the matter and gauge fields, where the latter are treated as unconstrained real variables. (We can write an explicit finitely defined statistical mechanics model that is properly sampled by such simulations, but do not belabor this because such details are not used here.)

In the  $\mathcal{J} = \infty$  models, we also use geometrical worm updates<sup>12,13</sup> of the discrete-valued conserved fluxes  $B$ . Where possible, we use multiple histogram method to interpolate between the data points;<sup>14</sup> the error bars are estimated by using blocking method and by running several independent samples.

As we change the parameters in the system, we monitor, first of all, thermal properties such as the specific heat per site  $C$ . This is defined through the variance of the action,

$$C = \frac{\langle (S - \langle S \rangle)^2 \rangle}{L^d}, \quad (12)$$

and can alert about phase transformations in the system even when we do not know the underlying physics. At a second-order phase transition,  $C$  behaves as  $C \sim |t - t_c|^{-\alpha} = |t - t_c|^{-(2-\nu d)}$ , where in the last equation we used the relation between the specific heat exponent  $\alpha$  and the correlation length exponent  $\nu$ . The singularity is rounded off in a finite system, but manifests itself as a peak in the specific heat that evolves characteristically with the system size. In a finite volume  $L^d$ , the peak location approaches the bulk critical point as  $t_{\text{peak}} - t_c \sim L^{-1/\nu}$ , while the peak height behaves as

$$C_{\text{max}} \sim C_0 + AL^{2/\nu-d}, \quad (\text{second order}). \quad (13)$$

For comparison, at a first order transition, the peak height grows with the system size as

$$C_{\text{max}} \sim L^d, \quad (\text{first order}), \quad (14)$$

which would be measured as  $\nu_{\text{eff}} = 1/d = 1/3$  in a naive analysis in 3D; the peak location converges to the bulk critical point as  $t_{\text{peak}} - t_c \sim L^{-d}$ .

Thus, the behavior of the specific heat gives first indication about the nature of the transition. In the NCCP<sup>0</sup> model, we anticipate a continuous transition with  $\nu \simeq 0.67$  – the exponent  $\alpha$  is then small and negative, and the singularity in  $C$  is only a cusp. In this case,  $C$  is less useful for scaling, but a good estimate of  $\nu$  can be obtained by studying the third cumulant of the action,<sup>15</sup>

$$C_3 = \frac{\langle (S - \langle S \rangle)^3 \rangle}{L^d}, \quad (15)$$

which can be viewed as a derivative of  $C$  with respect to a temperature-like parameter. Near the critical point, the characteristic  $C_3$  (such as the maximum value or the maximum - minimum difference) scales as  $L^{3/\nu-d}$ , which is more readily detected. This is useful in the NCCP<sup>1</sup> model as well, where, previewing the Monte Carlo results, the thermal signature of the transition is less singular and implies a larger exponent  $\nu$ .

Let us now consider direct detection of the Higgs transition. In the Higgs phase, the gauge field is massive and the fluxes do not fluctuate on large scales. On the other hand, in the Photon phase, the fluxes proliferate. This can be measured by what we call the dual stiffness

$$\rho_{\text{dual}}^{\mu\mu}(q) = \left\langle \frac{|\sum b_\mu(R) e^{iq \cdot R}|^2}{(2\pi)^2 L^3} \right\rangle. \quad (16)$$

Here the summation is over all plackets oriented perpendicular to  $\hat{\mu}$ ,  $b_\mu = (\nabla \times a)_\mu$  is the corresponding flux, and  $R$  is the coordinate of the placket. We consider the stiffness at a wavevector  $q$  and are interested in the small  $q$  limit. In an infinite system,  $\rho_{\text{dual}}$  is zero in the Higgs phase and is finite in the Photon phase. If the fluxes are viewed as conserved currents,  $\rho_{\text{dual}}$  is essentially the superfluid stiffness of this current loop system.

Recall also that in the NCCP<sup>0</sup> case at  $\mathcal{J} = \infty$ , the fluxes  $b/(2\pi)$  become integer-valued (the corresponding loops are the ANO vortex lines).  $\rho_{\text{dual}}$  is then precisely the conventional superfluid stiffness for this loop system (which also explains our normalization in Eq. 16). The loop model is usually studied with no restriction on the total flux, and one usually measures the stiffness at  $q = 0$ . This is not available in our setup: since we are working with the gauge fields and periodic boundary conditions, the total flux is constrained to be zero. However, we can measure the stiffness at a nonzero  $q \sim 1/L$ , and in the present work we use  $\rho_{\text{dual}}^{xx}$  and  $\rho_{\text{dual}}^{yy}$  at the smallest  $q_{\text{min}} = (0, 0, 2\pi/L)$ . In a finite system, this observable is less sharp than  $\rho_{q=0}$ . Thus, in the phase with only small loops, there is a contribution to  $\rho_q$  of order  $q^2 \sim 1/L^2$ , while the  $q = 0$  stiffness would vanish exponentially with  $L$ . Still, we find that this observable works well. The NCCP<sup>0</sup> model allows us to develop such experience and test our protocols before studying the NCCP<sup>1</sup> case.

At a second-order transition, we expect the product  $\rho_{\text{dual}}(q_{\text{min}}) \cdot L$  to be universal, while near criticality

$$\rho_{\text{dual}}(q_{\text{min}}; t, L) \cdot L = r(\delta L^{1/\nu}), \quad (17)$$

where  $\delta = t - t_c$  measures deviation from the critical point and  $r(x)$  is a scaling function. We plot the  $\rho_{\text{dual}} \cdot L$  curves and look at their crossings and thus estimate the location of the critical point. We also extract the correlation length exponent  $\nu$  by applying the above scaling form. We try different approaches. One is to consider a derivative with respect to a temperature-like parameter in the system (such derivatives can be calculated accurately in the Monte Carlo process). At the critical point we expect

$$\left. \frac{d(\rho_{\text{dual}} \cdot L)}{dt} \right|_{\text{crit}} \sim L^{1/\nu}, \quad (18)$$

which can be used to estimate  $\nu$ . This approach is sensitive to our uncertainty in the location of the critical point and is not very robust: e.g., the critical such curve does not separate the ones on the two sides of the transition but eventually should go above all of them. A different procedure is to consider the maximal value of the derivative for each  $L$ . Yet another approach is to scale the full  $\rho_{\text{dual}} \cdot L$  curves near criticality. We are using all such approaches, but a crude look at the derivatives is simple and will already be sufficient for our comparison of the NCCP<sup>0</sup> and NCCP<sup>1</sup> models – our main message will be that  $\nu$  is larger in the latter case.

The discussed thermal measures and the dual stiffness work in any matter-gauge system. In the NCCP<sup>1</sup> case,

we also have the field  $\vec{n}$ , Eq. (6), which is a local physical observable in the matter sector. We measure the magnetization associated with the O(3) ordering,

$$\vec{m} = \frac{1}{L^d} \sum_i \vec{n}_i, \quad (19)$$

and estimate the critical point from the crossings of the corresponding Binder cumulant ratio

$$g = \frac{\langle |\vec{M}|^4 \rangle}{\langle |\vec{M}|^2 \rangle^2}. \quad (20)$$

Similarly to Eq. (17), we expect the following scaling form near the critical point:

$$g(t, L) = g(\delta L^{1/\nu}), \quad (21)$$

which we analyze in the same spirit as the  $\rho_{\text{dual}} \cdot L$ .

We characterize the O(3) ordering by the magnetization exponent  $\beta$ :  $m \sim \delta^\beta$ . This gives the following finite-size scaling ansatz

$$m(t, L) = L^{-\beta/\nu} f(\delta L^{1/\nu}). \quad (22)$$

In particular, right at the critical point we expect

$$m|_{\text{crit}} \sim L^{-\beta/\nu} = L^{-(1+\eta)/2}, \quad (23)$$

where the last equation defines exponent  $\eta$  in 3D. By plotting  $m$  vs  $L$  on a log-log plot, the critical curve is a straight line that separates the curves on the ordered and disordered sides. This analysis independently checks the location of the critical point and gives an estimate of  $\beta/\nu$ .

Finally, we also observe the transition by monitoring the helicity modulus  $\Upsilon$  for twisting the O(3) vector field  $\vec{n}$ . This can be calculated in the standard way during the same Monte Carlo process, and we give detailed expressions for the two NCCP<sup>1</sup> models in Appendix B. The helicity modulus is also a measure of the ordering in the O(3) matter sector, but has a somewhat different character from the magnetization and is more like a superfluid stiffness in a boson system. The scaling of the helicity modulus at a second-order transition is similar to the dual stiffness described earlier. In particular, we expect universal crossings of the  $\Upsilon \cdot L$  curves, which is yet another way of locating the transition in our finite-size study. These measurements can also be compared with other studies of such matter-gauge systems,<sup>9</sup> and also with studies of quantum Hamiltonians whose critical behavior may be described by such field theories.<sup>4,5,6</sup>

## B. Representative study of the transitions in the three models at $\mathcal{K}=0.4$

Here we present Monte Carlo results at  $\mathcal{K} = 0.4$  in the three models. This is sufficiently away from the  $\mathcal{K} = \infty$

limit – for example, the critical coupling  $\mathcal{J}_c(\mathcal{K} = 0.4)$  is at least 50% larger than  $\mathcal{J}_c(\mathcal{K} = \infty)$  in each case:  $\mathcal{J}_c(0.4) = 0.682$  vs  $\mathcal{J}_c(\infty) = 0.4541$  in the NCCP<sup>0</sup> model;  $\mathcal{J}_c(0.4) = 1.412$  vs  $\mathcal{J}_c(\infty) = 0.9358$  in the NCCP<sup>1</sup> model I; and  $\mathcal{J}_c(0.4) = 1.68$  vs  $\mathcal{J}_c(\infty) = 0.98$  in the NCCP<sup>1</sup> model II. Furthermore, the transition is clearly observed in the behavior of the gauge field as detected by the dual stiffness – we see a convergence of the crossings of  $\rho_{\text{dual}} \cdot L$  for our system sizes. In the NCCP<sup>1</sup> models, we also see convergence of the Binder ratio crossings and the  $\Upsilon \cdot L$  crossings, which detect the transition in the matter sector. Recall that the gauge sector is completely absent in the  $\mathcal{K} = \infty$  limit, and indeed at large  $\mathcal{K}$  the “critical points” defined by the “gauge” and “matter” measures start far apart for our system sizes, but are already close at  $\mathcal{K} = 0.4$ . We expect comparable finite size effects in the three systems as far as the development of the true Higgs criticality is concerned.

We will discuss the observed trends along the Photon - Higgs phase boundary in Secs. III D, III E. The representative point  $\mathcal{K} = 0.4$  was chosen to be sufficiently away from the first-order region in the NCCP<sup>1</sup> model I, with the hope that it is not affected strongly by crossovers near the tricritical point. We argue here that the transition is continuous in all three models at  $\mathcal{K} = 0.4$ . In the NCCP<sup>0</sup> case, this is expected theoretically and is supported numerically. In all measured respects, the transition in either of the NCCP<sup>1</sup> models at  $\mathcal{K} = 0.4$  looks more continuous than NCCP<sup>0</sup>.

Figure 2 shows the specific heat per site in the three models. In each case, we see a peak whose position moves towards the estimated critical point and whose height increases gradually. The slow evolution of the position and the weak (at most sublinear) growth of  $C_{\text{max}}$  with the system size are indicative of the continuous nature of the transition and rather large correlation length exponent  $\nu$  in each case. Fitting  $C_{\text{max}}$  to Eq. (13), we estimate  $\nu \approx 0.65 - 0.7$  in the NCCP<sup>0</sup> case, which is close to the accepted value in the (inverted) 3D XY. We find a somewhat larger  $\nu \approx 0.70$  in the NCCP<sup>1</sup> model I case. In the NCCP<sup>1</sup> model II, the growth of the peak height with the system size is very weak and we do not attempt to analyze  $C_{\text{max}}$ . We also measure the third cumulant  $C_3$ , Eq. (15), and analyzing this data gives estimates of  $\nu$  consistent with the above. In the three systems at  $\mathcal{K} = 0.4$ , we do not see any tendency towards first order behavior such as Eq. (14). Furthermore, energy histograms for system sizes up to  $L = 36$  show one mode and no sign of any structure developing. From all such measures, the transition in the presented NCCP<sup>1</sup> systems has weaker thermal singularities than in the NCCP<sup>0</sup> case.

Let us describe how we locate the transitions more accurately. Figure 3 shows the crossings of  $\rho_{\text{dual}}(q_{\text{min}}) \cdot L$ , which approach the critical point from the opposite direction compared with the  $C_{\text{max}}$  positions. The crossings converge quickly for our system sizes and thus allow an accurate determination of  $\mathcal{J}_c$ .

In the NCCP<sup>1</sup> systems, we also observe the transition

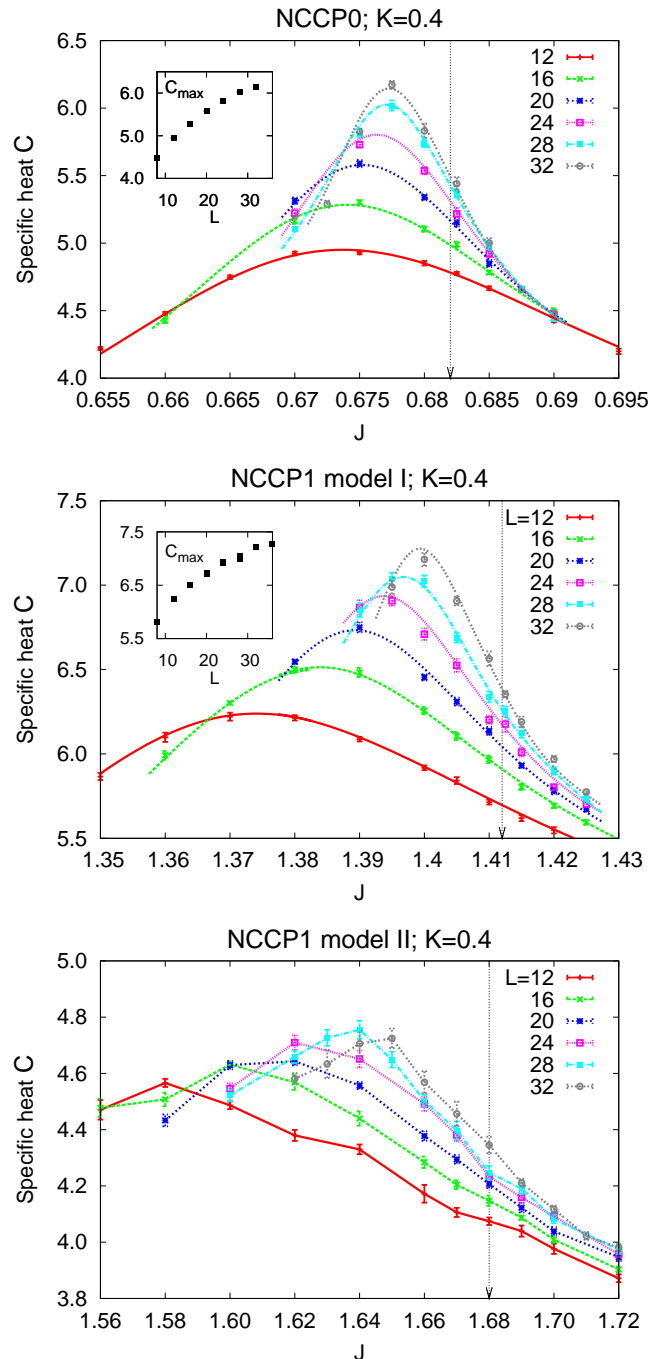


FIG. 2: (color online). Specific heat  $C$  in the three models at  $\mathcal{K} = 0.4$  varying  $\mathcal{J}$  near the transition. System sizes are  $L = 12 - 32$ . In the top and middle panels, the lines are obtained by multiple histogram method, which provides a systematic interpolation between data points; the corresponding peak values  $C_{\text{max}}$  are plotted in the insets and show sublinear growth with  $L$ . In the bottom panel, the lines are only guides to the eye connecting nearby data points; in this case, the peak value changes too little to be extracted reliably. In each panel, the vertical arrow shows the bulk critical point  $\mathcal{J}_c$  estimated from Figs. 3 and 4. The specific heat peak moves towards this point gradually and the developing singularity is weak, which is a direct evidence of the second-order nature of the transition.

directly in the matter sector by measuring the magnetization  $\bar{m}$ , Eq. (19). The corresponding Binder ratios are shown in Fig. 4 for the models I and II. Comparing with the appropriate panels in Fig. 3, we see that the Binder crossings move in the opposite direction to the  $\rho_{\text{dual}}(q_{\text{min}}) \cdot L$  crossings, and the two measures effectively bound the location of the transition to a narrow region.

Finally, Fig. 5 shows the crossings of  $\Upsilon \cdot L$  in the two NCCP<sup>1</sup> models, providing an alternative detection of the transition in the matter sector. The crossings converge towards the bulk critical point similarly to the Binder crossings and also help to bound the transition region.

Having estimated the critical points, let us now discuss scaling in the three models. In the panels in Figs. 3, 4, and 5, we also show the corresponding derivatives evaluated at points bounding the transition<sup>16</sup> vs the system size  $L$ . In each case, we perform simple linear fits corresponding to Eq. (18) on the log-log plot and list the extracted values of  $\nu$ . This procedure is not very reliable and does not necessarily bound the exponent, but it gives a crude picture of the results we obtain doing more elaborate scalings.

In the NCCP<sup>0</sup> case, such scalings of  $\rho_{\text{dual}}(q_{\text{min}}) \cdot L$  suggest  $\nu$  between 0.5 and 0.55, which we interpret as some effective value on our length scales. This is significantly different from the expected  $\nu \simeq 0.67$ , but when we look closer, we do see the corresponding plots curving in the direction of such larger  $\nu$ . Thus, naive scaling of  $\rho_{\text{dual}}(q_{\text{min}}) \cdot L$  in the one-component matter-gauge system at this  $\mathcal{K}$  suffers from strong finite size effects. We could in principle improve our estimates of  $\nu$  by performing more complex fits including corrections to scaling, but in the absence of good control over these, we do not venture in this direction. Instead, in the spirit of the comparative study, we should be prepared for similar effects also in the two-component system.

In the NCCP<sup>1</sup> model I, such scalings of  $\rho_{\text{dual}}(q_{\text{min}}) \cdot L$  show effective  $\nu$  between 0.55 and 0.65. This is larger than the effective  $\nu$  in the above NCCP<sup>0</sup> case, suggesting that the true  $\nu$  in the two-component system is larger than in the one-component system. From the scaling of the Binder ratio, of the  $\Upsilon \cdot L$ , and of other observables in the matter sector, we estimate  $\nu$  between 0.65 and 0.7 (somewhat smaller than the crude values in the top panel in Fig. 4), which further supports our proposal  $\nu_{\text{NCCP}^1} > \nu_{\text{NCCP}^0}$ . We warn, however, that our scalings in the model I at  $\mathcal{K} = 0.4$  may already be affected by the proximity of the Molecular phase – see the discussion of the trends along the Photon - Higgs phase boundary in Sec. III E.

Turning to the NCCP<sup>1</sup> model II, the scalings of  $\rho_{\text{dual}}(q_{\text{min}}) \cdot L$  consistently suggest  $\nu$  around 0.7 (somewhat larger than the crude estimates in the bottom panel in Fig. 3), while the scalings of the Binder ratio suggest  $\nu$  between 0.7 and 0.75. This system does not have any Molecular phase nearby and, being sufficiently away from the  $\mathcal{K} = \infty$  limit, is closer to the true two-component Higgs criticality than the model I. The  $\Upsilon \cdot L$  data in the

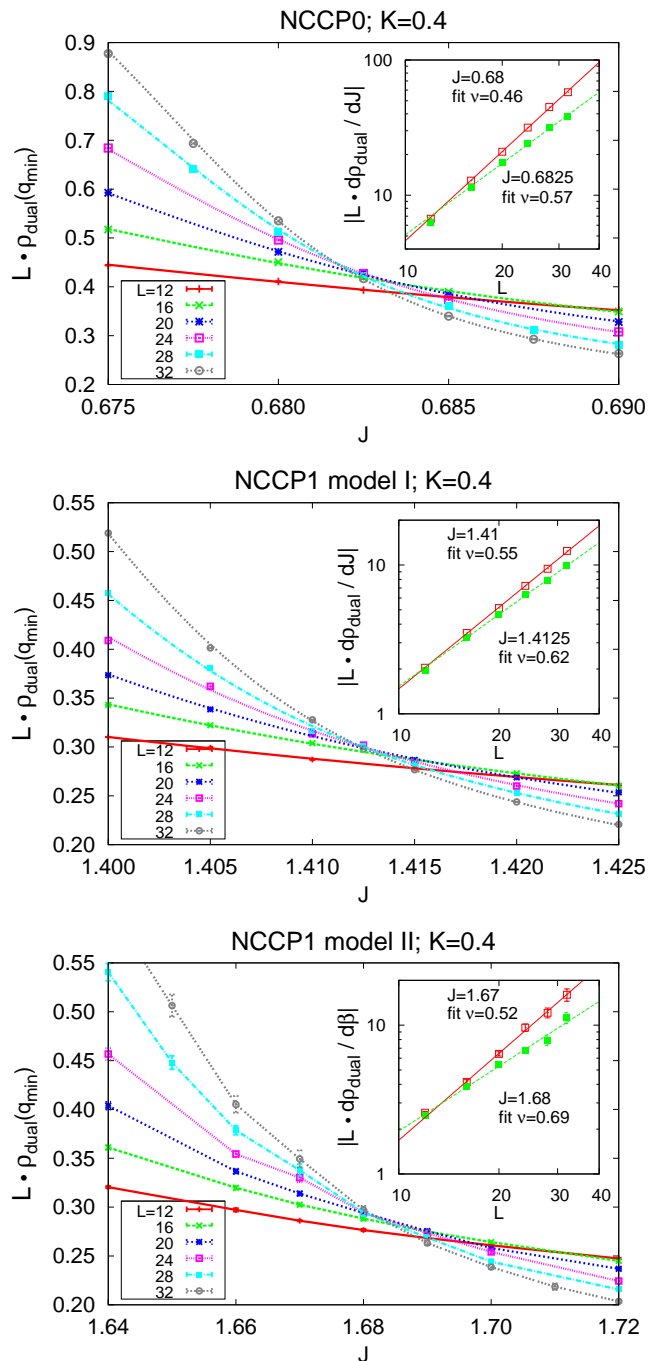


FIG. 3: (color online).  $\rho_{\text{dual}}(q_{\text{min}}) \cdot L$  in the three models at  $\mathcal{K} = 0.4$ . The crossings converge quickly towards  $\mathcal{J}_c = 0.682$  in the NCCP<sup>0</sup> model (top panel),  $\mathcal{J}_c = 1.412$  in the NCCP<sup>1</sup> model I (middle panel), and  $\mathcal{J}_c = 1.68$  in the NCCP<sup>1</sup> model II (bottom panel). In the last two cases, we can check the convergence against the Binder ratio crossings, Fig. 4, which move in the opposite direction. In each panel, the inset summarizes naive estimates of the correlation length exponent  $\nu$  applying Eq. (18) to the derivative data at points bordering the transition – see text for details.



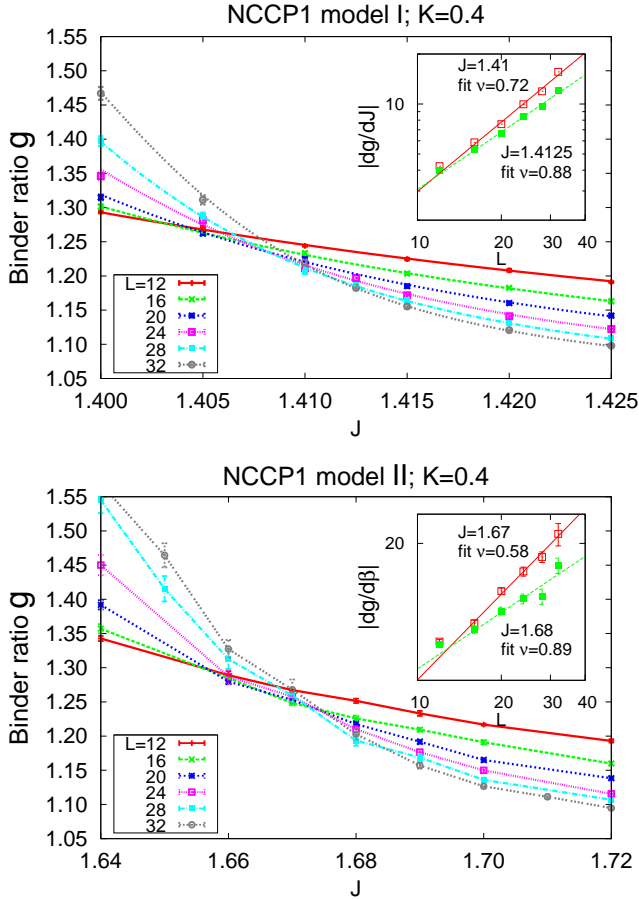


FIG. 4: (color online). Binder ratios in the NCCP<sup>1</sup> models I and II at  $\mathcal{K} = 0.4$ . The crossings bound the transition point from the opposite side compared with the  $\rho_{\text{dual}}(q_{\text{min}}) \cdot L$  crossings, Fig. 3. In the insets, we show naive estimates of  $\nu$  fitting the derivative of the Binder ratio to the form  $\sim L^{1/\nu}$  at points bordering the transition.

model II is rather noisy, as one see from the corresponding panel in Fig. 5. This model is harder to simulate than model I: e.g., we cannot use local heat bath updates of the matter fields and we cannot use multi-histogram reweighting; there is also significant complexity in the expression for  $\Upsilon$ , Eq. (B1). Still, we see that  $\Upsilon \cdot L$  shows reasonable crossings and is bounded by value of order 1 at criticality with no significant drifts. Here, it is helpful to have the bounds on the critical  $\mathcal{J}_c$  from the more accurate  $\rho_{\text{dual}} \cdot L$  and Binder crossings, Figs. 3 and 4, so there are no uncertainties where the  $\Upsilon \cdot L$  crossings might flow. We will describe overall trends along the phase boundary in the model II in Sec. III D.

Finally, from the magnetization scaling, we also estimate the exponent  $\eta$  in the two NCCP<sup>1</sup> models at  $\mathcal{K} = 0.4$ , finding it to be around  $0.4 - 0.5$  in both cases on our system sizes.

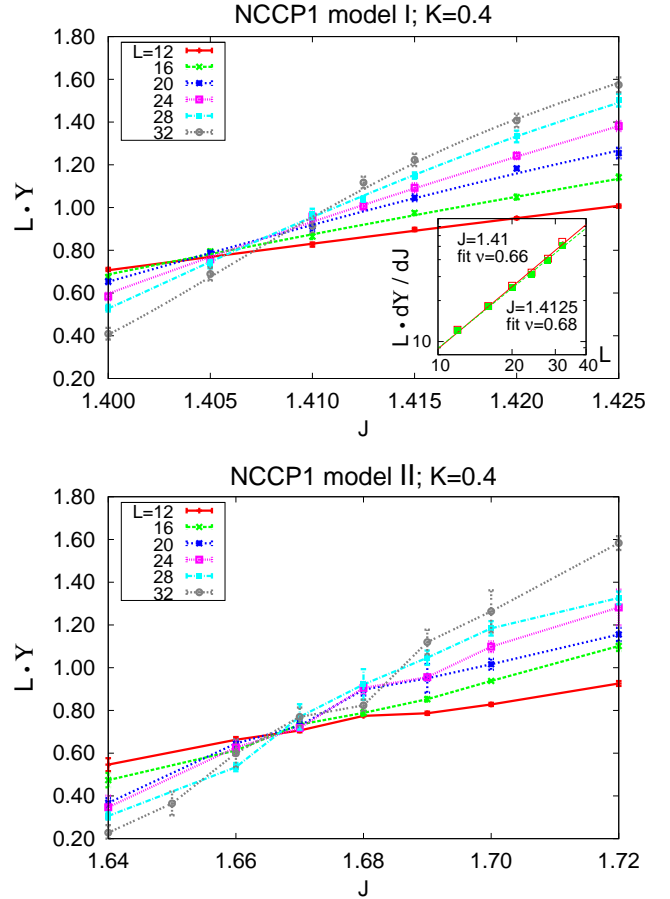


FIG. 5: (color online).  $\Upsilon \cdot L$  in the NCCP<sup>1</sup> models I and II at  $\mathcal{K} = 0.4$ . The crossings move in the same direction as the Binder ratio crossings, Fig. 4, and bound the transition point from the opposite side compared with the  $\rho_{\text{dual}}(q_{\text{min}}) \cdot L$  crossings, Fig. 3. The inset in the model I case shows scaling analysis of the derivative similar to the analysis in Fig. 3 (no such derivative data was measured in the model II).

### C. NCCP<sup>0</sup> model and NCCP<sup>1</sup> model II at $\mathcal{J} \rightarrow \infty$

Before describing overall trends along the Photon - Higgs phase boundary in the three models, we present Monte Carlo results in the two  $\mathcal{J} = \infty$  models, Eqs. (7) and (10). In our simulations, we also use geometrical worm updates<sup>12,13</sup> of the discrete-valued conserved fluxes  $B$ . This eliminates the critical slowing down in the NCCP<sup>0</sup> case and significantly improves statistics in the NCCP<sup>1</sup> case. In the latter, we still use local updates of the matter fields, which is probably why the critical slowing down persists.

As we have already described, the NCCP<sup>0</sup> model at  $\mathcal{J} = \infty$  is equivalent to the well-studied loop model with short-range interactions. We use it to develop experience with the  $\rho_{\text{dual}}(q_{\text{min}}) \cdot L$  to characterize the transition, and we find that this measure works well. The study also allows us to connect with the points measured along the phase boundary in the NCCP<sup>0</sup> model at finite  $\mathcal{J}$ ,

Fig. 1a, gaining experience with finite size effects in such matter-gauge simulations – we will use this when discussing overall trends in Sec. III D. Furthermore, we can now compare the two  $\mathcal{J} = \infty$  models Eqs. (7) and (10) directly.

In Fig. 6, we show the specific heat  $C$  in the two models. In the NCCP<sup>0</sup> case, there is a clear peak which moves towards the bulk critical point and sharpens slowly with increasing system size. Analyzing the thermal singularity as in Sec. III B and as described in Eqs. (12)–(15), we obtain an estimate of the correlation length  $\nu = 0.66 - 0.67$ , which is in agreement with the accepted value  $\nu = 0.67$ . Turning to the NCCP<sup>1</sup> case, the specific heat signature of the transition is weaker and appears as a feature that develops on top of a sloping down background. The evolution of the feature with  $L$  is more slow than in the NCCP<sup>0</sup> case, implying a larger exponent  $\nu$ . From the study of the third cumulant of the action, we estimate  $\nu \simeq 0.75 - 0.8$ .

Let us now characterize the transitions using the dual stiffness shown in Fig. 7. In either case, we see a rapid convergence of the  $\rho_{\text{dual}}(q_{\text{min}}) \cdot L$  crossings towards the putative bulk critical point. In the NCCP<sup>0</sup> model, the crossing for the largest two systems  $L = 28$  and  $32$  occurs around  $\mathcal{K} = 0.07609$ , very close to the true  $\mathcal{K}_c = 0.07606$ , and the crossing location is still moving slightly in the expected direction. In the inset, we show the derivative  $d(\rho_{\text{dual}} \cdot L)/d\mathcal{K}$  as a function of  $L$  at two points  $\mathcal{K}$  that bound the critical point; direct fits give  $\nu_{\text{fit}}(\mathcal{K} = 0.0760) = 0.62$  and  $\nu_{\text{fit}}(\mathcal{K} = 0.0761) = 0.73$ , which in turn bound the expected  $\nu$ . As discussed in Secs. III A and III B, the inset should be viewed only as a crude illustration of the scaling analysis, but it is already sufficient for our comparative study.

Proceeding with similar analysis in the NCCP<sup>1</sup> case shown in the bottom panel in Fig. 7, the critical point is between  $\mathcal{K} = 0.1240$  and  $0.1245$ . From the analysis in the inset, we estimate  $\nu$  between  $\nu_{\text{fit}}(\mathcal{K} = 0.1240) = 0.68$  and  $\nu_{\text{fit}}(\mathcal{K} = 0.1245) = 0.80$ . More elaborate scaling procedures suggest that  $\nu$  is between  $0.7$  and  $0.75$ . The correlation length exponent is thus detectably larger than in the NCCP<sup>0</sup> case.

In the NCCP<sup>1</sup> case, we also consider the Binder ratio, Fig. 8. The crossings of  $g$  bound the critical point from the opposite side compared with the  $\rho_{\text{dual}} \cdot L$  crossings. Performing finite size scaling analysis of the Binder ratio curves gives estimates of  $\nu$  between  $0.7$  and  $0.8$ , which is consistent with the presented other estimates.

Finally, in Fig. 9, we show finite size scaling analysis of the magnetization. We plot  $m(\mathcal{K}, L)$  as a function of  $L$  at fixed  $\mathcal{K}$ , expecting Eq. (23) at the critical point. In the figure, there is a clear separation between the magnetically ordered and disordered sides, and from the fits at the test points we estimate  $\eta$  between  $\eta_{\text{fit}}(\mathcal{K} = 0.1240) = 0.29$  and  $\eta_{\text{fit}}(\mathcal{K} = 0.1245) = 0.18$ . Since the Binder ratios, which detect the criticality in the matter sector, still cross near  $\mathcal{K} = 0.1240$  for our largest systems, the correspond value of  $\eta$  is likely closer to the

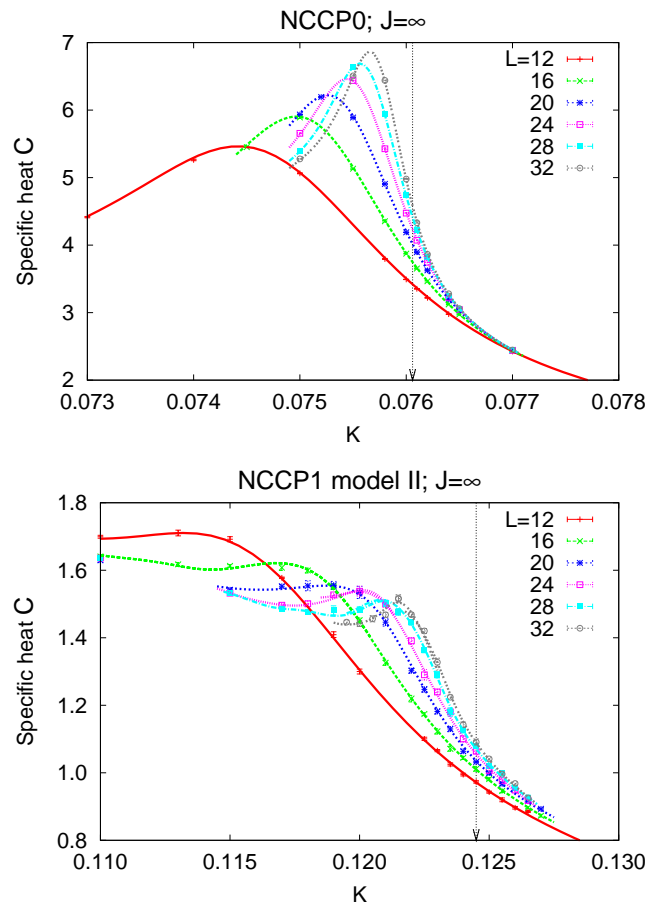


FIG. 6: (color online). Top panel: Specific heat in the NCCP<sup>0</sup> model at  $\mathcal{J} = \infty$ , Eq. (7). This is the same as a loop model with steric interactions in an ensemble with no windings. Bottom panel: Specific heat in the NCCP<sup>1</sup> model II at  $\mathcal{J} = \infty$ , Eq. (10). In each panel, the connecting lines are obtained by multiple histogram method; the vertical arrow shows the bulk critical point  $\mathcal{K}_c$  estimated from Figs. 7 and 8. The NCCP<sup>1</sup> transition sharpens more slowly with  $L$  than NCCP<sup>0</sup> and is characterized by a larger exponent  $\nu$ .

true exponent. When we try to scale the full magnetization curves near criticality, we get a somewhat wider range of  $\eta = 0.2 - 0.4$ .

To summarize, the transition in the NCCP<sup>1</sup> model II at  $\mathcal{J} = \infty$  has a weaker thermal singularity than in the NCCP<sup>0</sup> model; it is a second-order transition with  $\nu_{\text{NCCP}^1} > \nu_{\text{NCCP}^0}$ . This conclusion is also supported by the scaling analysis of the  $\rho_{\text{dual}} \cdot L$  and of the Binder ratios, which give

$$\nu = 0.7 - 0.75, \quad (\text{NCCP}^1 \text{ model II, } \mathcal{J} = \infty). \quad (24)$$

The magnetization order is characterized by the exponent

$$\eta = 0.2 - 0.4, \quad (\text{NCCP}^1 \text{ model II, } \mathcal{J} = \infty). \quad (25)$$

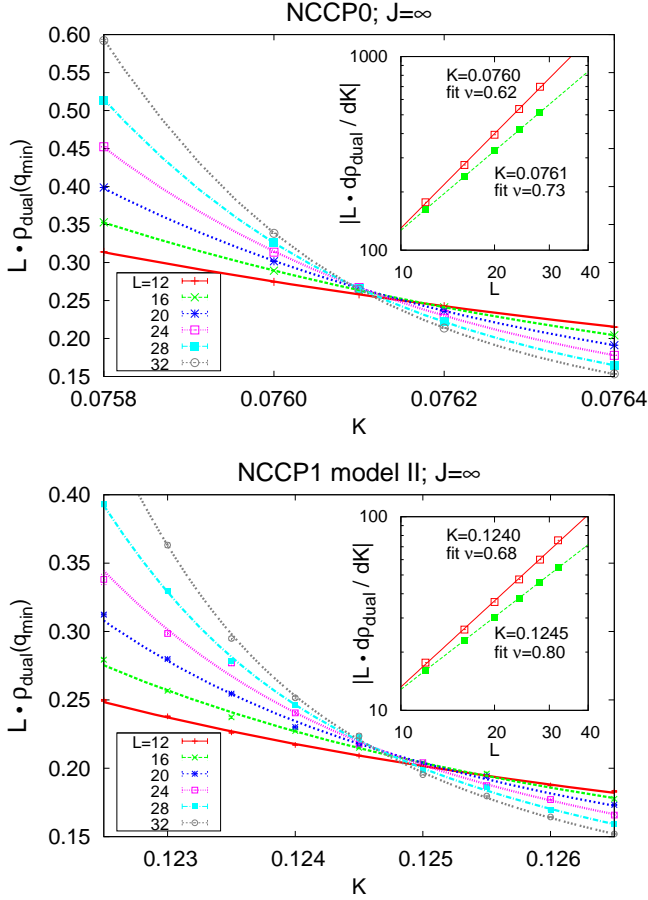


FIG. 7: (color online). Top panel:  $\rho_{\text{dual}}(q_{\text{min}}) \cdot L$  in the NCCP<sup>0</sup> model at  $\mathcal{J} = \infty$ . The critical point is known accurately to be  $\mathcal{K}_c = 0.07606$  ( $\nu = 0.67$ ), and the crossings converge rapidly to this location. Inset shows the derivative of  $\rho_{\text{dual}} \cdot L$  with respect to  $\mathcal{K}$  as a function of  $L$  at two test points that bound the critical region; the lines are direct fits to the form  $\sim L^{1/\nu}$ , and the corresponding estimates of  $\nu$  are also listed. Bottom panel: Similar analysis in the NCCP<sup>1</sup> model II at  $\mathcal{J} = \infty$ ; our best estimate for  $\mathcal{K}_c$  is  $\mathcal{K}_c \approx 0.1245$ .

### 1. $\Upsilon \cdot L$ in the NCCP<sup>1</sup> model II at large $\mathcal{J} = 16$

We have not been able to measure the helicity modulus  $\Upsilon$  directly in the NCCP<sup>1</sup> model II at  $\mathcal{J} = \infty$ : One expression for the  $\Upsilon$  that we derived in this limit contained singular integrals over the  $z$  variables and was ill suited for the Monte Carlo sampling integration. Instead, we performed a study at large but finite  $\mathcal{J} = 16$  and measured the expression Eq. (B1). This is our closest connection with the  $\mathcal{J} = \infty$  limit tracking the behavior of  $\Upsilon \cdot L$  along the phase boundary in Fig. 1c. The horizontal  $\mathcal{J} = 16$  cut is very far from the decoupled  $\mathcal{K} = \infty$  limit and also far from the vertical  $\mathcal{K} = 0.4$  cut presented in Sec. III B. Nevertheless, the measured  $\Upsilon \cdot L$  crossings on the two cuts are rather similar, illustrating that there is no significant flow of the critical  $\Upsilon \cdot L$  values along the phase boundary.

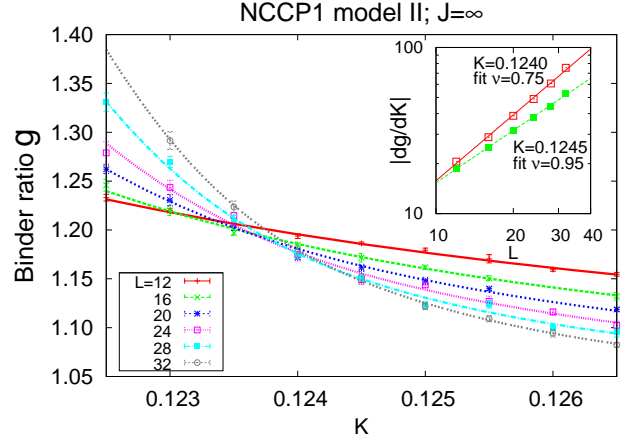


FIG. 8: (color online). Binder ratio  $g$  in the NCCP<sup>1</sup> model II at  $\mathcal{J} = \infty$ . Comparing with the corresponding  $\rho_{\text{dual}} \cdot L$  plot in Fig. 7, the  $g$  crossings converge to the same critical point bounding it from the opposite side. Inset shows estimates of  $\nu$  from the analysis of the derivative of  $g$ , in the same spirit as in Fig. 7.

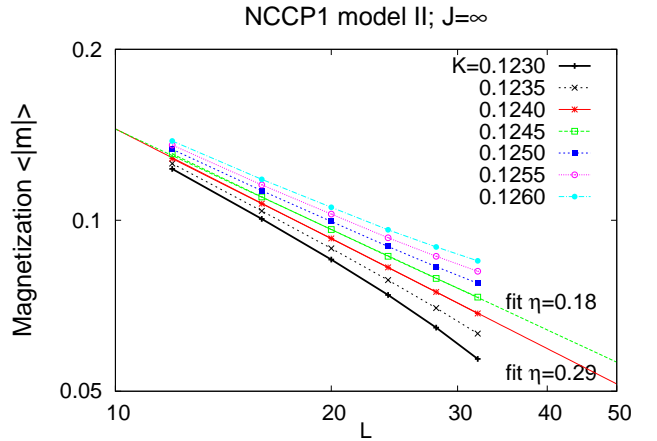


FIG. 9: (color online). Finite size scaling analysis of the magnetization. We expect  $m \sim L^{-(1+\eta)/2}$  at criticality and perform fits for the exponent  $\eta$  at two test points. On the log-log plot, the ordered and disordered sides curve up and down respectively, confirming the estimates of the critical region from Figs. 7 and 8.

The  $\mathcal{J} = 16$  study is summarized in Fig. 10. The  $\rho_{\text{dual}}(q_{\text{min}}) \cdot L$  crossings and the Binder ratio crossings behave similarly to the  $\mathcal{J} = \infty$  model, Figs. 7 and 8. These measures, which have smooth limits for large  $\mathcal{J}$ , have clean statistics and allow us to accurately constrain the critical point to lie between  $\mathcal{K} = 0.132$  and  $0.1325$ . On the other hand, the  $\Upsilon \cdot L$  data is much more noisy: Individual terms present in Eq. (B1) can have large typical values and large cancellations are to occur upon the full integration. Still, we see that the  $\Upsilon \cdot L$  values near the criticality have not changed significantly from the  $\mathcal{K} = 0.4$  cut in Fig. 5, despite the much larger value of  $\mathcal{J}$  here.

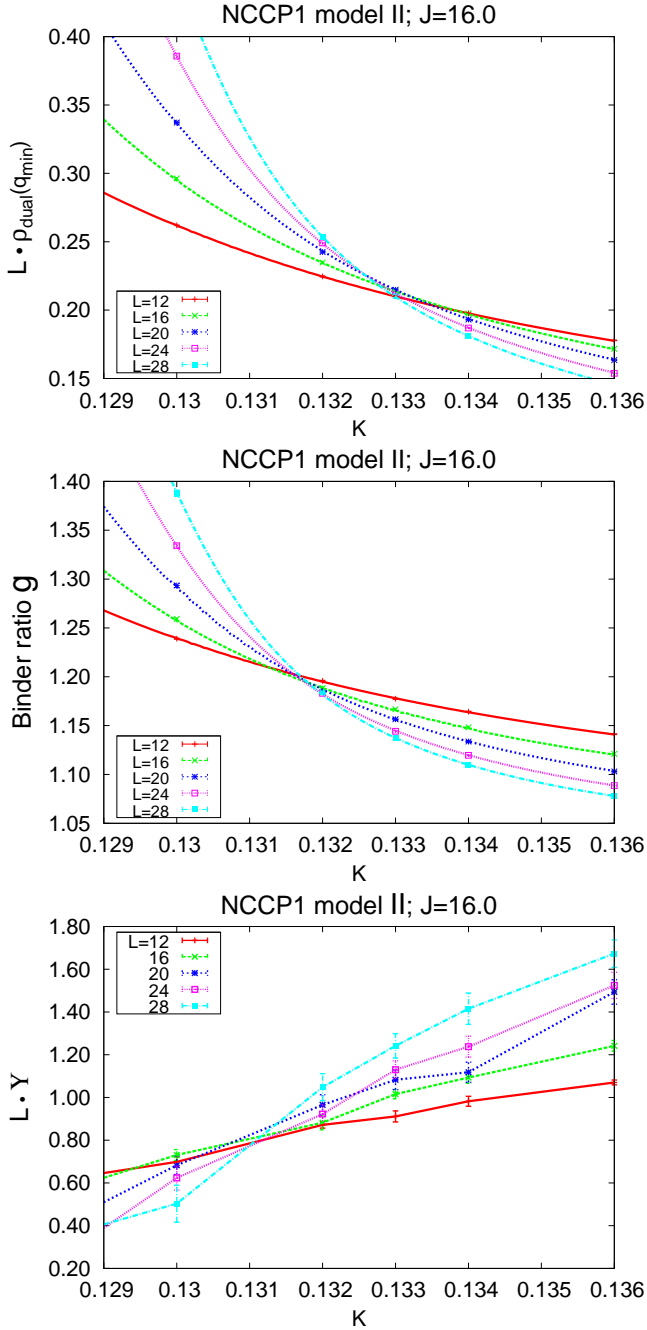


FIG. 10: (color online) Universal crossings in the NCCP<sup>1</sup> model II at large  $J = 16$ . This is our closest approach towards  $\mathcal{J} = \infty$ , and the focus here is on the boundedness of the  $\Upsilon \cdot L$  at criticality. In the top and middle panels,  $\rho_{\text{dual}}(q_{\text{min}}) \cdot L$  crossings move towards smaller  $\mathcal{K}$  values and the Binder ratio crossings move towards larger  $\mathcal{K}$  values, localizing the transition between  $\mathcal{K} = 0.132$  and  $0.1325$ . The  $\Upsilon \cdot L$  data in the bottom panel is noisy, but it is bounded by a value close to 1 and is similar to the  $\Upsilon \cdot L$  crossings at other cuts across the phase boundary in Fig. 1c (compare, e.g., with the vertical cut at  $\mathcal{K} = 0.4$  shown in Fig. 5). In the top and middle panels, where the data quality is good, the interpolating lines are obtained by the multi-histogram reweighting technique, while in the bottom panel the lines connect the individual data points; the error bars are estimated by averaging over different Monte Carlo runs.

#### D. Qualitative summary of the full Photon - Higgs phase boundary in the NCCP<sup>0</sup> model and NCCP<sup>1</sup> model II

We now summarize Monte Carlo results along the Photon - Higgs phase boundary in each of the three models. The phase diagrams were mapped out using the same criticality locators as in the preceding sections. Small systems up to  $L = 16 - 20$  were sufficient to get good estimates of the transition points marked in Fig. 1, while several points were studied up to  $L = 24 - 32$  and with detail comparable to Secs. III B, III C.

Specifically, in the NCCP<sup>0</sup> model and in the NCCP<sup>1</sup> model II, we studied a vertical cut at  $\mathcal{K} = 0.25$  and a horizontal cut at  $\mathcal{J} = 4$ , cf. Figs. 1a,c. Combined with the study of the  $\mathcal{J} = \infty$  limit, we thus observed the full evolution of our measurements along the phase boundary in the two models. Some details will be given shortly, but we can already say that in either model the criticality at different places along the phase boundary is qualitatively similar to the presented  $\mathcal{K} = 0.4$  case and connects smoothly to the  $\mathcal{J} = \infty$  limit. From all studies, the  $\mathcal{J} = \infty$  models are probably closest to the desired Higgs universalities, being least affected by other fixed points. In particular, these models provide our best estimates of the critical indices. We also studied in detail the phase boundary in the NCCP<sup>1</sup> model I, where the situation is more complicated – we will return to this model in the next section.

First, we give some details in the NCCP<sup>0</sup> case. The transitions are detected using the  $\rho_{\text{dual}} \cdot L$  crossings and look qualitatively similar to the  $\mathcal{K} = 0.4$  case presented in Sec. III B and the  $\mathcal{J} = \infty$  case in Sec. III C. The locations of the crossings converge quickly to the critical point. On the other hand, the specific heat peak evolves slowly with the system size and moves towards the bulk critical point as in the top panels of Figs. 2 and 6.

One observation that we make is that the values of  $\rho_{\text{dual}} \cdot L$  at the crossings, while apparently converged, are different at different locations along the phase boundary – compare, for example, the top panels of Figs. 3 and 7 – which is at first disconcerting. However, the observed values at the crossings approach those at  $\mathcal{J} = \infty$  as we move towards this point along the phase boundary. We believe that in the thermodynamic limit,  $\rho_{\text{dual}} \cdot L$  is universal at criticality. Indeed, we can show that our dual stiffness in the one-component matter-gauge system is equal to a sum of a stiffness  $\rho$  of a mathematically equivalent discrete-valued current loop model with short-range interactions and of a positive contribution of order  $1/(\mathcal{J}L^2)$ . Then, assuming universal  $\rho \cdot L$  at criticality in discrete loop models, the  $\rho_{\text{dual}} \cdot L$  crossings in the NCCP<sup>0</sup> model must converge to the same value but with a positive finite-size correction of order  $1/(\mathcal{J}L)$ , which is indeed comparable to the magnitude of the difference between the  $\rho_{\text{dual}} \cdot L$  values in Figs. 3 and 7. We note also that in the NCCP<sup>0</sup> model at  $\mathcal{K} = 0.4$ , the initial drift of the  $\rho_{\text{dual}} \cdot L$  value at the crossings upon increasing our

system sizes is actually away from the  $\mathcal{J} = \infty$  value, but we expect that this drift will eventually turn back. While we do not have full understanding of all such finite-size effects in our systems, the smooth evolution along the phase boundary and our analytical understanding make us confident in the proposed inverted 3D XY universality in the NCCP<sup>0</sup> model. It is also useful to note that such corrections will have much smaller effect on the rapid convergence of the locations of the crossings to the bulk critical point, which is indeed what we observe.

Concluding with the NCCP<sup>0</sup> case, the scaling analysis of the dual stiffness as in Sec. III B yields effective  $\nu$  that starts around 0.5-0.55 for  $\mathcal{K} = 0.4$  and moves towards the expected value  $\nu = 0.67$  as we approach  $\mathcal{J} = \infty$ , adding to our confidence that we understand this system well.

Let us now provide similar details for the NCCP<sup>1</sup> model II, whose phase diagram has the same topology as in the NCCP<sup>0</sup> case. Here again we see no qualitative difference in the observed criticality as we move along the phase boundary from the  $\mathcal{K} = 0.4$  point to the  $\mathcal{J} = \infty$ . For example, the specific heat peaks evolve slowly to the bulk critical points as in Figs. 2 and 6. The peak heights  $C_{\max}$  in the vertical cut at  $\mathcal{K} = 0.25$  and in the horizontal cut at  $\mathcal{J} = 4.0$  are essentially size-independent, i.e., they look even less sharp compared to the  $\mathcal{K} = 0.4$  case. Using  $\rho_{\text{dual}} \cdot L$  to detect the criticality, the picture that we observe is also very similar to the NCCP<sup>0</sup> model. In particular, since the two systems are simulated under similar finite size conditions, it is likely that similar effects are responsible for the apparent difference in the  $\rho_{\text{dual}} \cdot L$  values at the crossings as we move along the phase boundary. In this respect, the NCCP<sup>0</sup> model, which we otherwise understand well, provides a useful reference on such effects that we still don't have much experience with. This gives us confidence when interpreting the NCCP<sup>1</sup> case, which is our main focus.

In the NCCP<sup>1</sup> model, we also observe the transition using the ordering of  $\vec{n}$ , which monitors the matter sector. In a broad view of the phase diagram, Fig. 1c, for large  $\mathcal{K}$  the Binder ratio crossings and the  $\rho_{\text{dual}} \cdot L$  crossings start far apart for our system sizes, but as we move along the phase boundary towards smaller  $\mathcal{K}$ , the separation in the apparent criticality in the two sectors decreases significantly. Recall that the gauge sector is absent in the  $\mathcal{K} = \infty$  limit. The convergence of such locators of the criticality in both sectors shows that the system is sufficiently away from the  $\mathcal{K} = \infty$  limit and we are indeed probing the true Higgs universality.

At points between  $\mathcal{K} = 0.4$  and  $\mathcal{J} = \infty$ , scaling analyses of both the  $\rho_{\text{dual}} \cdot L$  and the Binder ratio give us consistently  $\nu$  in the range 0.7 to 0.75, supporting the conclusion that we are dealing with the same continuous transition for all points on the phase boundary in this model. Finally, our study of the helicity modulus also agrees well with the  $\rho_{\text{dual}} \cdot L$  and Binder ratio measurements. Thus, the  $\Upsilon \cdot L$  crossings agree with the other locators of the criticality. Furthermore, everywhere on the phase boundary, we find roughly similar values  $\Upsilon \cdot L \approx 1$

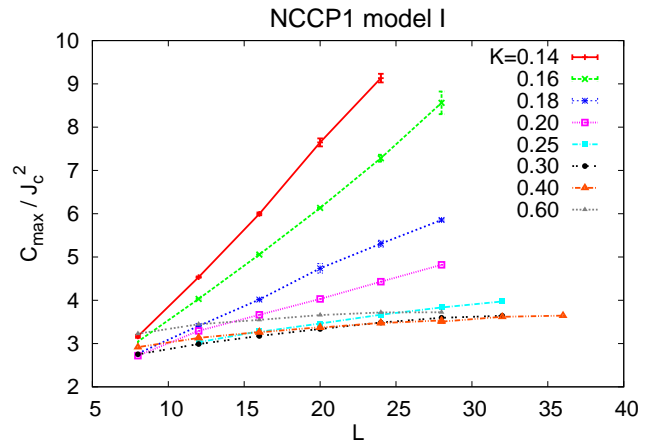


FIG. 11: (color online). Peak height of the specific heat in the NCCP<sup>1</sup> model I measured at different locations along the Photon - Higgs phase boundary, cf. Fig. 1b. The data at  $\mathcal{K} = 0.4$  is the same as in the corresponding inset in Fig. 2. We remove the overall scale of the action by plotting  $C_{\max}/\mathcal{J}_c^2$ , where  $\mathcal{J}_c$  is the critical value for a given  $\mathcal{K}$ . Similar plot in the NCCP<sup>1</sup> model II (not shown) has  $C_{\max}$  that depends very weakly on  $L$  for all points along the phase boundary in Fig. 1c.

at criticality, including the cut at  $J = 16$  presented in Sec. III C 1, which is the largest  $\mathcal{J}$  for which the  $\Upsilon$  was measured. There is no significant flow of the critical  $\Upsilon \cdot L$  values along the phase boundary in the NCCP<sup>1</sup> model II, consistent with the same continuous transition everywhere as implied by all other measures.

### E. Qualitative summary of the full Photon - Higgs phase boundary in the NCCP<sup>1</sup> model I

Let us now discuss the NCCP<sup>1</sup> model I. Fig. 11 summarizes our measurements of the thermal properties along the Photon - Higgs boundary, cf. Fig. 1b. For  $\mathcal{K} \geq 0.25$ , the specific heat peak height  $C_{\max}$  grows weakly with  $L$  – at most sublinearly for our system sizes. For  $\mathcal{K} = 0.18 - 0.20$ , the growth is linear, and becomes faster and dramatic for smaller  $\mathcal{K}$ . Note that in Fig. 11 we have divided  $C_{\max}$  by the corresponding  $\mathcal{J}_c^2$  thus removing crudely the overall scale, so it is reasonable to compare the magnitudes among the different  $\mathcal{K}$  data. The  $\rho_{\text{dual}} \cdot L$  crossings, Binder cumulant crossings, and  $\Upsilon \cdot L$  crossings are already well converged for these system sizes (cf. the  $\mathcal{K} = 0.4$  data in Sec. III B), i.e., these systems are far from the  $\mathcal{K} = \infty$  limit and represent fully coupled matter-gauge criticalities. Our interpretation of the thermal signatures is that the transition is second-order for  $\mathcal{K} > 0.2$  and is first order for  $\mathcal{K} < 0.2$ , while  $\mathcal{K} \approx 0.2$  is a candidate for the tricritical point separating the two behaviors. (It is worth repeating here that a similar  $C_{\max}$  plot in the model II, where there is no Molecular phase, has essentially size-independent  $C_{\max}$  for all points along the phase boundary.)

The transition at  $\mathcal{K} = 0.3$  appears more sharp compared to the  $\mathcal{K} = 0.4$  point presented in Sec. III B, and various broad-brush scaling analyses give a smaller  $\nu_{\text{eff}}(\mathcal{K} = 0.3, L \leq 32) \approx 0.6$ . The transition appears still more sharp at  $\mathcal{K} = 0.2$  with  $\nu_{\text{eff}} \approx 0.5$ . Also, the effective exponent  $\eta$  for the magnetization order parameter decreases towards zero as we approach  $\mathcal{K} = 0.2$ . For  $\mathcal{K} = 0.25, 0.3$ , we observe that the extracted  $\nu$  and  $\eta$  tend to increase slightly when the scaling range around the critical point is made more narrow. We interpret the apparent exponent drift along the phase boundary to be due to crossovers near the tentative tricritical point near  $\mathcal{K} = 0.2$ . (To repeat here, we see no such exponent drift in the model II).

Certainly, this drift is an important concern that we have been unable to fully address in the model I with our system sizes. These difficulties are the main reason why we also considered the NCCP<sup>1</sup> model II, where the first order region is absent and the systematics of the scalings is improved, as we have already described. This experience with the model II gives us better grounds for making the above interpretation in the model I. It would be useful to confront this with direct simulations in the model I on larger system sizes than in our work. Larger systems should allow one to better filter out the crossovers and focus on the true critical behavior, e.g., confronting our expectation of the universal exponents along the continuous region of the phase boundary.

To give more details behind the proposed scenario in the NCCP<sup>1</sup> model I, we also present the behavior of the Binder ratio crossings and  $\Upsilon \cdot L$  crossings along the Photon - Higgs phase boundary. These are vital locators of the criticality and are expected to converge to universal values in the second-order case. Going back to Figs. 4 and 5 at  $\mathcal{K} = 0.4$ , we see some weak evolution of the values at the crossings. We find that these values further drift as we move along the phase boundary. Similarly to the drifts in the apparent exponents, this is an important concern. In this regard, it is helpful to have a picture of all data along the phase boundary. We can then try to see possible attracting points of such drifts of the crossings and also see where the presented detailed study at  $\mathcal{K} = 0.4$  of Sec. III B stands in the overall picture.

The top panel in Fig. 12 summarizes all collected data for the Binder ratio crossings. For each  $\mathcal{K}$ , we consider a vertical  $\mathcal{J}$  scan across the phase boundary in Fig. 1b and analyze the Binder ratios as done in Fig. 4. For each pair of system sizes  $L_1$  and  $L_2$ , we find the corresponding crossing of the curves and organize the results by showing  $\{\sqrt{L_1 L_2}, g_{\text{cross}}(L_1, L_2; \mathcal{K})\}$ . Admittedly, the plot Fig. 12 is noisy, since the crossings are fairly sensitive to the statistical errors. For some systems we show results obtained from several independent data samples, so the spread of the symbols gives some idea about our uncertainties. Generally, we do not trust the values when the crossings become non-systematic with  $L$ , which happens for our largest systems. From the available data, we see that for  $\mathcal{K} > 0.2$  the Binder ratio values evolve

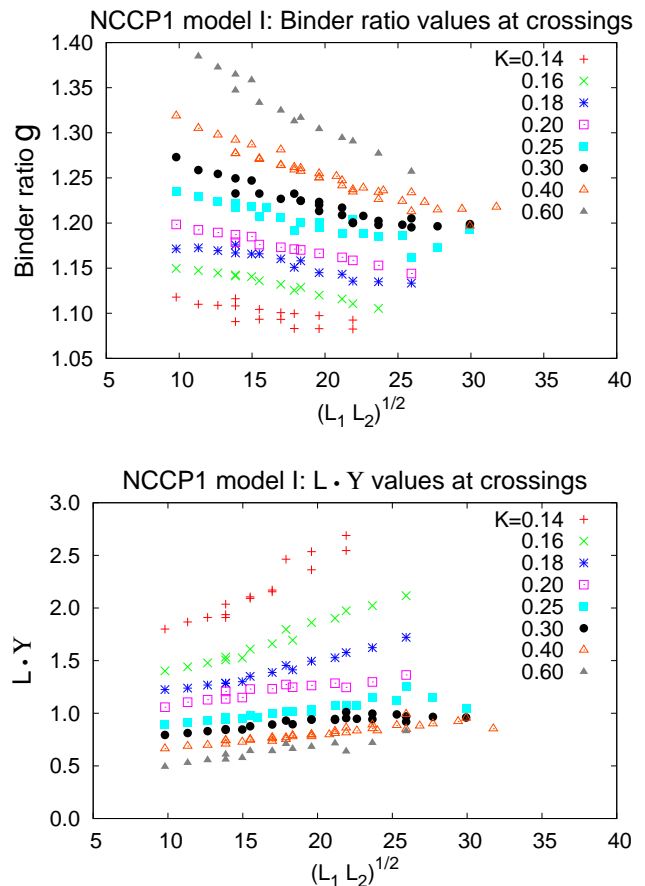


FIG. 12: (color online). Top panel: Binder ratio values at the corresponding crossings for all pairs of system sizes  $L_1$  and  $L_2$ . The data is collected by analyzing  $\mathcal{J}$  scans such as Fig. 4 at a number of  $\mathcal{K}$  locations along the Photon - Higgs phase boundary from Fig. 1b. For an illustration, the pairs of system sizes are organized by  $\sqrt{L_1 L_2}$  on the horizontal axis. Bottom panel:  $\Upsilon \cdot L$  values at the corresponding crossings obtained by analyzing the helicity modulus plots such as Fig. 5. Together with Fig. 13 and all other data, our interpretation is that the transition is continuous for  $\mathcal{K} > 0.2$  and becomes first order for  $\mathcal{K} < 0.2$ .

strongly initially but then appear to saturate to a value  $g \approx 1.2$  for the largest systems. On the other hand, for  $\mathcal{K} < 0.2$  the Binder ratios at the crossings flow to smaller values.

Note that in the scenario with the tricritical point, we expect that the Binder ratios go to different nontrivial values in each of the three cases – at the second-order line, at the tricritical point, and at the first-order transitions. In this respect, the fact that the initial evolution in all cases is in the same direction makes the interpretation of the Binder crossings data more difficult. Certainly, improving the statistics of the data in Fig. 12 and going to larger sizes could address such concerns and confront our interpretation, which we nevertheless make given all available data.

A more clear separation between the different regimes

is provided by similarly collected data for the  $\Upsilon \cdot L$  crossings shown in the bottom panel in Fig. 12. In the second-order case, we expect the crossings to go to a universal value, and we see that for  $\mathcal{K} > 0.2$  these indeed appear to accumulate to a value  $\Upsilon \cdot L \approx 1$  for the largest systems. On the other hand, in the first-order regime, we expect the  $\Upsilon \cdot L$  crossing values to increase linearly with the system sizes, and we indeed see such growth for  $\mathcal{K} < 0.2$ . We are fairly confident that in the proposed second-order region the values of  $\Upsilon \cdot L$  do not grow without limit at the transition, since we can bound the possible drift of the  $\Upsilon \cdot L$  crossing locations by the  $\rho_{\text{dual}} \cdot L$  crossing locations that converge to the transition from the opposite side, cf. Figs. 3, 4, and 5. (We repeat here that the  $\Upsilon \cdot L$  crossings in the NCCP<sup>1</sup> model II were also found to be bounded and of order 1 at several different places along the phase boundary; the situation in the proposed second-order regime in the NCCP<sup>1</sup> model I is consistent with this in the NCCP<sup>1</sup> model II.)

In Fig. 13, we present a somewhat different perspective on the collected Binder ratio,  $\Upsilon \cdot L$ , and  $\rho_{\text{dual}} \cdot L$  data. For each  $\mathcal{K}$ , we define an operational critical point  $\mathcal{J}_c(L)$  for a given size  $L$  as the point where the Binder ratio takes value  $g = 1.15$ . We then measure  $\Upsilon \cdot L$  and  $\rho_{\text{dual}} \cdot L$  at this point and plot the results as a function of  $L$ . The specific value  $g = 1.15$  lies between the apparent crossing values in the  $\mathcal{K} > 0.2$  and  $\mathcal{K} < 0.2$  regimes and is selected so that  $\mathcal{J}_c(L)$  approaches the true critical point systematically from the large  $\mathcal{J}$  values when  $\mathcal{K} > 0.2$ . Any  $g$  between the limits on the two sides of the transition can be used for such a definition of the finite-size critical point, and we have checked that the results do not change qualitatively if we fix the Binder ratio at different values such as  $g = 1.3, 1.2, 1.1$  instead.

From the top panel in Fig. 13, we see that thus measured  $\Upsilon \cdot L$  values hardly change with the system size for  $\mathcal{K} > 0.2$  and all are in a narrow range around 1.2 – 1.3. There may be slight systematic drift, and the ultimate fate of this is hard to judge given the uncertainties of our measurements and limited system sizes. However, we note that the relative variations of the  $\Upsilon \cdot L$  values are small: Had we chosen the vertical axis in the figure to start at zero, which is natural given that there is no other scale for the expected universal values of  $\Upsilon \cdot L$ , the curves for  $\mathcal{K} > 0.2$  would look essentially flat. Moreover, the values are fairly close in a whole range range  $\mathcal{K} = 0.25 - 0.6$ , and are also similar to the values we find at this Binder ratio in the NCCP<sup>1</sup> model II along the whole phase boundary (e.g., near points  $\mathcal{K} = 0.4, 0.25$  and  $\mathcal{J} = 4.0, 16.0$  in Fig. 1c). This is to be contrasted with the behavior for  $\mathcal{K} < 0.2$ , where we see a strong growth of the critical  $\Upsilon \cdot L$  with the system size starting from the small  $L$ , which is interpreted as first-order behavior.

Similar considerations apply to the  $\rho_{\text{dual}} \cdot L$  measured at fixed  $g = 1.15$  and shown in the bottom panel in Fig. 13. For  $\mathcal{K} < 0.2$ , the  $\rho_{\text{dual}} \cdot L$  values grow strongly with the system size, while for  $\mathcal{K} > 0.2$  they grow very

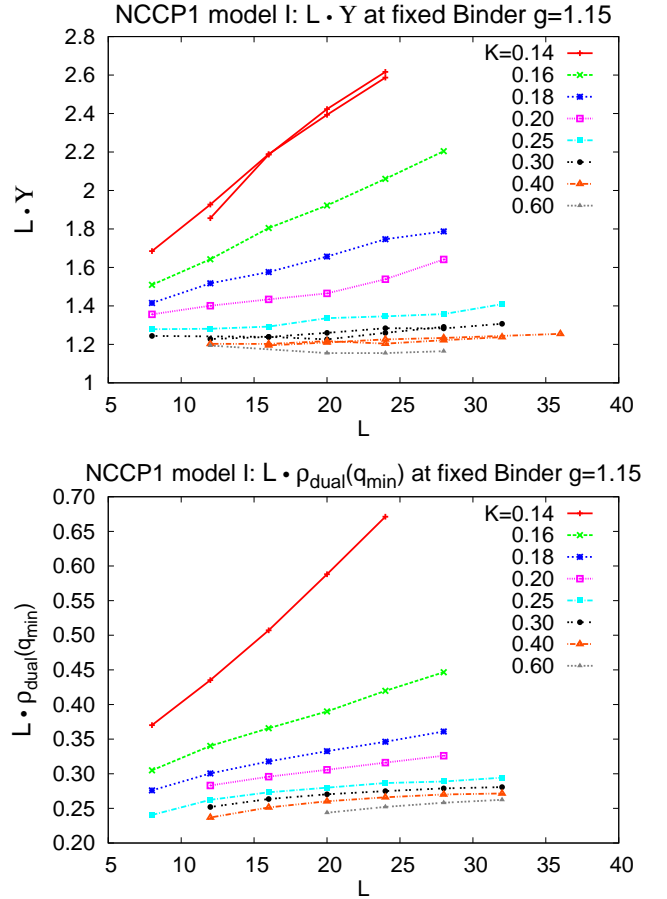


FIG. 13: (color online). Different view of the Binder ratio,  $\Upsilon \cdot L$ , and  $\rho_{\text{dual}} \cdot L$  data. For each system size, we define the finite-size critical point to be where the Binder ratio takes value  $g = 1.15$  and then measure the  $\Upsilon \cdot L$  and  $\rho_{\text{dual}} \cdot L$  at this point and plot the results as a function of  $L$ . Our interpretation of the data is that the transition is continuous for  $\mathcal{K} > 0.2$  and becomes first order for  $\mathcal{K} < 0.2$ .

weakly and tend to saturate. We should mention that we do not see such clear separation between the two regimes by looking at the pairwise crossings of  $\rho_{\text{dual}} \cdot L$  (not shown): The values at the crossings are essentially size-independent for all  $\mathcal{K}$  for our sizes, i.e., we do not see the first order region in this measure yet. We also want to point out that from the study of the model II at  $\mathcal{J} = \infty$ , Fig. 7, we expect the critical value of  $\rho_{\text{dual}} \cdot L$  to be eventually smaller than what we see at the crossings in the model I. That is, there are strong finite size corrections to this measure, but such tendencies are similar to what we have observed in the NCCP<sup>0</sup> model and NCCP<sup>1</sup> model II and discussed earlier.

We have also analyzed the evolution of the extracted  $\eta$  exponent in the two NCCP<sup>1</sup> models along the phase boundary. In the model II, we see a convergence with the system size towards the value  $\eta \approx 0.3$  estimated in the  $\mathcal{J} \rightarrow \infty$  limit, cf. Eq. (25). On the other hand, the effective  $\eta$  is still larger around 0.4-0.5 in the model I

at  $\mathcal{K} = 0.6, 0.4$  for our system sizes but is decreasing. The initial large effective  $\eta$  is expected, given that this ‘Molecular’ order parameter has  $\eta \approx 1.37$  at the  $O(4)$  point<sup>17</sup> where the matter and gauge fields are decoupled. This also explains why the original small system study of the NCCP<sup>1</sup> model I at  $\mathcal{K} = 0.6$  in Ref. 2 obtained large  $\eta$ , which we now revise.

To conclude, despite some uncertainties with the weak drifts as we move along the Photon - Higgs phase boundary in the NCCP<sup>1</sup> model I, we believe that there is a wide regime where the transition is continuous. While the discussion of the full phase boundary is sketchy (in particular, we have not tried to accurately characterize the tricritical and first-order regimes), it provides better understanding of possible issues and concerns in our numerical explorations of the Higgs transition, and, in particular, gives a better idea where the detailed study at  $\mathcal{K} = 0.4$  of Sec. IIIB stands in the overall picture. We conclude that  $\mathcal{K} = 0.4$  is well inside the continuous regime; recall that it is also far from the  $\mathcal{K} = \infty$  limit, so we have strong reasons to claim that it is representative of the true continuous Higgs criticality.

#### IV. SUMMARY AND CONCLUSIONS

To summarize, we perform a comparative Monte Carlo study of the Higgs transition in the one-component and two-component lattice superconductors and argue for the generic second-order nature in both cases. The one-component model (called NCCP<sup>0</sup> here), which is well understood analytically and numerically, serves as a reference system for our matter-gauge simulations.

We first examine in detail the two-component model introduced in Ref.<sup>2</sup> and called NCCP<sup>1</sup> model I here. The phase diagram is shown in Fig. 1b, and we argue that there is a range of parameters,  $\mathcal{K} > 0.2$ , where the transition is second-order. The main evidence is the weakness of the thermal singularities, but other measures are also in favor of the second-order nature. We present an example of such an analysis at  $\mathcal{K} = 0.4$  and argue that the correlation length exponent is larger than in the NCCP<sup>0</sup> case.

The NCCP<sup>1</sup> model I also has the Molecular phase. In the vicinity where the three phases meet, the thermal signatures of the Photon to Higgs transition change dramatically, see Fig. 11. We interpret this as the transition becoming first order for  $\mathcal{K} < 0.2$ , which is also expected on general grounds due to increasing fluctuations of the molecular field, see Appendix A. This interpretation implies a tricritical point around  $\mathcal{K} \approx 0.2$  separating the two regimes.

It is difficult to characterize firmly the region of continuous transitions in the model I. At each point, scaling apparently works, but the extracted exponents drift as we move along the phase boundary, with both  $\nu$  and  $\eta$  decreasing towards 0.5 and 0 respectively as we approach  $\mathcal{K} = 0.2$ . We attribute this to crossovers near the tricriti-

cal point. In this picture, the second-order region is bordered by the  $O(4)$  transition at  $\mathcal{K} = \infty$  and the tricritical point near  $\mathcal{K} = 0.2$ . The RG flows near the corresponding fixed points are causing a wealth of crossovers. The absence of full leverage over such phenomena is the main source of our difficulties in this model. It is worth repeating that in this picture the Higgs transition is controlled by a new fixed point, and there is no contradiction here since the RG flows are likely occurring in a more complex space than just the  $\mathcal{K} - \mathcal{J}$  parameter space of the specific model. By studying the dual stiffness and comparing with the NCCP<sup>0</sup> model, we know that our systems are sufficiently away from the  $\mathcal{K} = \infty$  limit, and the apparently continuous transition with large  $\nu$  is most naturally explained as the second-order Higgs universality.

To alleviate the difficulties associated with the crossovers near the putative tricritical point, we also consider a modification of the original NCCP<sup>1</sup> model by adding short-range antiferromagnetic interactions that hinder the formation of the Molecular phase. In fact, in the specific NCCP<sup>1</sup> model II, the Molecular phase is eliminated completely, allowing one to focus solely on the Photon to Higgs transition. We find that the transition is continuous along the whole phase boundary, see Fig. 1c. The scalings are consistent throughout, giving the large correlation length exponent. The transition line connects smoothly with the  $\mathcal{J} = \infty$  limit, which can be viewed as a description in terms of the Abrikosov-Nielsen-Olesen vortices that have nontrivial internal structure. We are able to realize this structure and study the transition in Monte Carlo using local matter degrees of freedom, and this numerics gives our best estimates of the critical indices  $\nu$  and  $\eta$ , Eqs. (24) and (25). For the future, it would be useful if one could realize such a nontrivial loop system in a manner that would eliminate critical slowing down, as is possible for the ANO vortices of the one-component model, which are short-range interacting loops with no internal structure.

Let us conclude with more questions that one would like to study. First of all, we mention possible applications to unusual quantum critical phenomena in magnets.<sup>3,5,6</sup> Our correlation length and magnetization exponents are broadly in agreement with those found in the study of the continuous Neel to Valence Bond Solid transition in an  $SU(2)$  symmetric spin-1/2 system in Refs. 5,6. (It would also be useful to compare universal amplitudes as discussed in Ref. 18.) Motivated by this application, it would be useful to find the scaling dimension of a monopole insertion operator in the gauge theory Eq. (1), since this corresponds<sup>3</sup> to the VBS order parameter measured in Ref.<sup>5,6</sup>. Our  $\mathcal{J} = \infty$  formulation of the model II, where inserting a monopole (antimonopole) corresponds to a source (sink) for the discrete  $B$ -fluxes, may be well suited for this. It would also be useful to find the scaling dimension of multiple monopole insertions. For example, one would like to check whether quadrupled monopoles are irrelevant as proposed in the deconfined criticality scenario for the Neel - VBS transition on the



square lattice and as needed for the non-compact gauge theory Eq. (1) to be applicable to this transition.<sup>3</sup>

It would be also useful to know the effect of various deformations away from the SU(2)-invariant case. For example, recently Alet *et al.*<sup>7</sup> studied a Coulomb to Valence Bond Solid transition in a classical dimer model on a 3D cubic lattice. This can be (approximately) mapped<sup>19</sup> to Eq. (1) plus cubic anisotropy terms, which, however, appear only with more derivatives/fields. Alet *et al.*<sup>7</sup> found a continuous transition but with different critical indices from ours. Several possible explanations are given in Ref. 7, and more studies would be worthwhile.

Finally, we would also like to revisit the  $U(1) \times U(1)$  variant using the insights learned here.

### Acknowledgments

We have benefited from useful discussions with M. P. A. Fisher, D. Huse, T. Senthil, and A. B. Kuklov. The numerical work was started at KITP, and use of the Hewlett-Packard and CNSI Computer Facilities at UCSB is gratefully acknowledged. The numerical work at Caltech was performed using the IT2 computer system operated by the Caltech CACR. A.V. acknowledges support from NSF DMR-0645691 and O.I.M. from the A. P. Sloan Foundation.

### APPENDIX A: MEAN FIELD ANALYSIS NEAR THE MOLECULAR PHASE

Here we summarize the mean field argument that in the two-component system, the Photon to Higgs transition becomes first order in the vicinity of the Molecular phase.<sup>9</sup> We introduce an order parameter  $\vec{N}$  for the molecular phase and write a schematic Landau theory that contains all three phases:

$$S[\Psi, \vec{N}] = m_\psi |\Psi|^2 + \frac{u_\psi}{2} |\Psi|^4 + m_N \vec{N}^2 + \frac{u_N}{2} (\vec{N}^2)^2 - g \vec{N} \cdot \Psi^\dagger \vec{\sigma} \Psi. \quad (\text{A1})$$

Setting  $u_\psi = u_N = g = 1$  and minimizing this action, we obtain the phase diagram in Fig. 14. Away from the fork all transitions are continuous, while near the fork the Photon to Higgs and Molecular to Higgs transitions become first order. Let us see how this happens for the Photon to Higgs transition. For large positive  $m_N$ , we can “integrate out” the  $\vec{N}$  field and obtain the renormalization  $u_\psi \rightarrow u_\psi - g^2/(2m_N)$ . When we approach the

Molecular phase,  $m_N$  becomes smaller leading to a sign change for the  $|\Psi|^4$  term. By the familiar mechanism in the Landau theory, the transition becomes first order due to such short-distance energetics near the molecular phase.

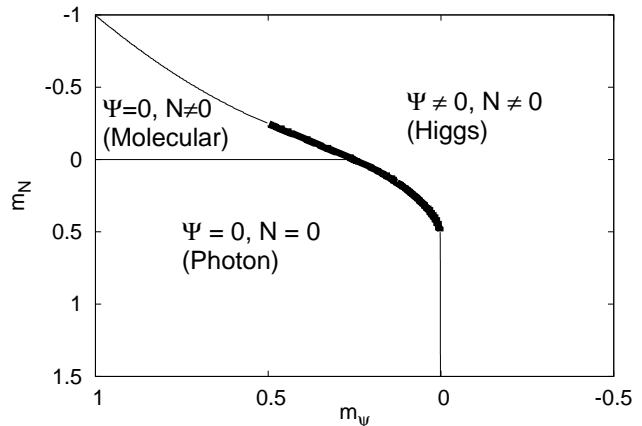


FIG. 14: Phase diagram of the Landau mean field theory Eq. (A1) in the vicinity where the three phases meet. The bold lines mark where the transitions become first order in the vicinity of the fork. We chose the axes so that  $m_\psi, m_N > 0$  in the lower left corner, which gives the locations of the phases roughly similar to that in Fig. 1b.

### APPENDIX B: EVALUATION OF THE HELICITY MODULUS $\Upsilon$ IN THE NCCP<sup>1</sup> MODELS

The helicity modulus is defined from the dependence of the free energy on the twist in the boundary conditions. As is common when calculating stiffnesses in Monte Carlo, the twist angle can be distributed into small twists throughout the system, and the helicity modulus can be then obtained by measuring appropriate derivative expressions during simulations with periodic boundary conditions. In this approach, the expressions to be evaluated depend on the detailed interactions and are different in the NCCP<sup>1</sup> model I and model II cases.

Specifically, we consider twisting the vector  $\vec{n} = (n_1, n_2, n_3)$  in the  $n_1 - n_2$  plane, which is achieved by the substitution  $(z_{r\uparrow}, z_{r\downarrow}) \rightarrow (z_{r\uparrow} e^{i\gamma r_\mu}, z_{r\downarrow} e^{-i\gamma r_\mu})$  in the action for the twist imposed in the lattice direction  $\hat{\mu}$ . Carrying through the derivations, we can summarize the expressions to be measured in the two models as

$$\begin{aligned}
\Upsilon_\mu L^d &= \sum_i \mathcal{J} \left\langle \text{Re}[z_i^\dagger z_{i+\hat{\mu}} e^{ia_{i\mu}}] \right\rangle \\
&- \sum_i 4\mathcal{J}^2 \left\langle f(\mathcal{J}|z_i^\dagger z_{i+\hat{\mu}}|) \text{Re}[z_{i\uparrow}^* z_{i\downarrow} z_{i+\hat{\mu},\downarrow}^* z_{i+\hat{\mu},\uparrow}] \right\rangle + \sum_i 4\mathcal{J}^4 \left\langle g(\mathcal{J}|z_i^\dagger z_{i+\hat{\mu}}|) (\text{Im}[z_{i\uparrow}^* z_{i\downarrow} z_{i+\hat{\mu},\downarrow}^* z_{i+\hat{\mu},\uparrow}])^2 \right\rangle \\
&- \left\langle \left( \sum_i \mathcal{J} \text{Im}[z_{i\uparrow}^* z_{i+\hat{\mu},\uparrow} e^{ia_{i\mu}} - z_{i\downarrow}^* z_{i+\hat{\mu},\downarrow} e^{ia_{i\mu}}] - \sum_i 2\mathcal{J}^2 f(\mathcal{J}|z_i^\dagger z_{i+\hat{\mu}}|) \text{Im}[z_{i\uparrow}^* z_{i\downarrow} z_{i+\hat{\mu},\downarrow}^* z_{i+\hat{\mu},\uparrow}] \right)^2 \right\rangle, \quad (\text{B1})
\end{aligned}$$

where we introduced two functions  $f(x)$  and  $g(x)$ . In the model I case,  $f(x) = g(x) = 0$ . In the model II case, they are

$$f(x) = \frac{I_1(x)}{xI_0(x)}, \quad g(x) = \frac{f'(x)}{x}, \quad (\text{B2})$$

where  $I_0(x)$  and  $I_1(x)$  are the modified Bessel functions; the corresponding terms in the expression for  $\Upsilon$  arise from the additional interactions defining the model II, Eq. (5).

- 
- <sup>1</sup> B. I. Halperin, T. C. Lubensky, and Shang-keng Ma, Phys. Rev. Lett. **32**, 292 (1974).  
<sup>2</sup> O. I. Motrunich and A. Vishwanath, Phys. Rev. B **70**, 075104 (2004).  
<sup>3</sup> T. Senthil, A. Vishwanath, L. Balents, S. Sachdev, and M. P. A. Fisher, Science **303**, 1490 (2004); T. Senthil, L. Balents, S. Sachdev, A. Vishwanath, and M. P. A. Fisher, Phys. Rev. B **70**, 144407 (2004).  
<sup>4</sup> A. W. Sandvik, S. Daul, R. R. P. Singh, and D. J. Scalapino, Phys. Rev. Lett. **89**, 247201 (2002); A. W. Sandvik and R. G. Melko, Ann. Phys. (N.Y.) **321**, 1651 (2006).  
<sup>5</sup> A. W. Sandvik, Phys. Rev. Lett. **98**, 227202 (2007).  
<sup>6</sup> R. G. Melko and R. K. Kaul, Phys. Rev. Lett. **100**, 017203 (2008).  
<sup>7</sup> F. Alet, G. Misguich, V. Pasquier, R. Moessner, and J. L. Jacobsen, Phys. Rev. Lett. **97**, 030403 (2006); G. Misguich, V. Pasquier, and F. Alet, arXiv:0803.2196.  
<sup>8</sup> C. Dasgupta and B. I. Halperin, Phys. Rev. Lett. **47**, 1556 (1981).  
<sup>9</sup> A.B. Kuklov, N.V. Prokof'ev, B.V. Svistunov, and M. Troyer, Ann. Phys. (N.Y.) **321**, 1602 (2006).  
<sup>10</sup> S. Kragset, E. Smorgrav, J. Hove, F. S. Nogueira, and A. Sudbo, Phys. Rev. Lett. **97**, 247201 (2006); J. Smiseth, E. Smorgrav, E. Babaev, and A. Sudbo, Phys. Rev. B **71**, 214509 (2005).  
<sup>11</sup> F.-J. Jiang, M. Nyfeler, S. Chandrasekharan, and U.-J. Wiese, arXiv:0710.3926.  
<sup>12</sup> N. Prokof'ev and B. Svistunov, Phys. Rev. Lett. **87**, 160601 (2001).  
<sup>13</sup> F. Alet and E. S. Sorensen, Phys. Rev. E **68**, 026702 (2003).  
<sup>14</sup> M. E. J. Newman and G. T. Barkema, *Monte Carlo Methods in Statistical Physics*, Oxford University Press (1999).  
<sup>15</sup> A. Sudbo, E. Smorgrav, J. Smiseth, F. S. Nogueira, and J. Hove, Phys. Rev. Lett. **89**, 226403 (2002).  
<sup>16</sup> The derivatives in the insets in Figs. 3, 4, and 5 are calculated in the Monte Carlo process. In the NCCP<sup>0</sup> model and the NCCP<sup>1</sup> model I, the derivative is with respect to the parameter  $\mathcal{J}$  that multiplies the link energy, while in the NCCP<sup>1</sup> model II the derivative is with respect to a formal parameter  $\beta$  that would multiply the full energy (this derivative is less costly to compute and such different choices have little effect on the extracted exponents). We have not calculated the derivative of the helicity modulus  $\Upsilon$  in the NCCP<sup>1</sup> model II because of the complexity of the expression Eq. (B1) for the  $\Upsilon$  itself.  
<sup>17</sup> S. V. Isakov, T. Senthil, and Y. B. Kim, Phys. Rev. B **72**, 174417 (2005).  
<sup>18</sup> R. K. Kaul and R. Melko, arXiv:0804.2279.  
<sup>19</sup> D. L. Bergman, G. A. Fiete, and L. Balents, Phys. Rev. B **73**, 134402 (2006).